ornl

NUREG/CR-2996
ORNL/TM-8549

OAK RIDGE
NATIONAL
LABORATORY

MARTIN MARIETTA

Sensitivity of Detecting In-Core Vibrations and Boiling in Pressurized Water Reactors Using Ex-Core Neutron Detectors

Frank J. Sweeney
John-Paul A. Renier

Prepared for the
U.S. Nuclear Regulatory Commission
Office of Nuclear Regulatory Research
Under Interagency Agreement DOE 40-551-75

OPERATED BY
MARTIN MARIETTA ENERGY SYSTEMS, INC.
FOR THE UNITED STATES
DEPARTMENT OF ENERGY

Printed in the United States of America. Available from
National Technical Information Service
U.S. Department of Commerce
5285 Port Royal Road, Springfield, Virginia 22161

Available from

GPO Sales Program
Division of Technical Information and Document Control
U.S. Nuclear Regulatory Commission
Washington, D.C. 20555

NUREG/CR-2996
ORNL/TM-8549
NRC Distribution R4

Instrumentation and Controls Division

SENSITIVITY OF DETECTING IN-CORE VIBRATIONS AND BOILING IN PRESSURIZED WATER REACTORS USING EX-CORE NEUTRON DETECTORS

Frank J. Sweeney
John-Paul A. Renier*

Manuscript Completed: January 1984

Date Issued: July 1984

*Nuclear Engineering Applications Department,
Martin Marietta Computer Sciences Division.

Prepared for the
U.S. Nuclear Regulatory Commission
Office of Nuclear Regulatory Research
and
Office of Nuclear Reactor Regulation
Washington, DC 20555
under Interagency Agreement
DOE 40-551-75

NRC FIN No. B0191 and B0754

Prepared by the
OAK RIDGE NATIONAL LABORATORY
Oak Ridge, Tennessee 37831
operated by
MARTIN MARIETTA ENERGY SYSTEMS, INC.
for the
U.S. DEPARTMENT OF ENERGY
under Contract No. DE-AC05-840R21400

CONTENTS

CONTENTS (continued)

LIST OF FIGURES

LIST OF FIGURES (continued)

LIST OF FIGURES (Continued)

LIST OF FIGURES (Continued)

LIST OF TABLES

ABSTRACT

Neutron transport and diffusion theory space- and energy-dependent reactor kinetics calculations were performed in the frequency domain to determine the sensitivity of an ex-core neutron detector to in-core vibrations and coolant boiling in a pressurized water reactor (PWR). The results of these calculations indicate that the ex-core detectors are sensitive to neutron sources, to vibrations, and to boiling occurring over large regions of the core.

Calculations were also performed to determine the effects of fuel burnup, boron concentration, and xenon poisoning on the spatial sensitivity of the ex-core detector. These calculated results show that fuel assembly vibrations would be expected to produce ~60% greater ex-core detector response at the end of the first fuel cycle at Sequoyah-1 compared to the beginning of the fuel cycle for a constant amplitude of vibration.

The results were compared with experimental ex-core neutron noise data obtained from Sequoyah-1 during the first fuel cycle. The predicted increase in ex-core neutron noise was experimentally observed in the 2.5- to 4.0-Hz frequency range (the range of frequencies associated with fuel assembly vibration), indicating that the vibrational amplitude of the fuel assemblies did not increase significantly during the first fuel cycle.

1. INTRODUCTION

Ex-core neutron detector signals contain both steady-state (mean or dc) and stochastic (random) fluctuating components. These random (noise) signals have been used successfully to identify malfunctions of in-vessel components in pressurized water reactors (PWRs).[1-7] The main advantage of using noise analysis rather than other techniques to detect malfunctions is that existing instrumentation can be utilized to observe inherent system fluctuations without disturbing normal plant operation. Therefore, surveillance of ex-core neutron detector noise provides a simple, continuous, nonperturbative indirect means of monitoring the mechanical and thermal-hydraulic performance of reactor internals over the plant's operating life in an environment where appropriate instrumentation may not be installed (i.e., in-core accelerometers).

In order to provide surveillance and diagnosis of malfunctions, analysts must be able to relate changes in the neutron noise signal to changes in the reactor system. While ex-core detector neutron noise resulting from core barrel motion has been studied extensively,[1-6,8,9] the methodology for relating changes in the neutron noise caused by in-core perturbations such as fuel assembly vibration or coolant boiling has not been well developed. Also, in many cases observed changes in the ex-core neutron noise over a fuel cycle are not understood.

Methodologies for inferring the magnitude of fuel assembly vibrations or core coolant boiling are of great interest to PWR manufacturers[10,11] and to the U.S. Nuclear Regulatory Commission,[12,13] since excessive mechanical motion of fuel assemblies has led to fuel rod cladding failure in a number of PWRs.[14] The loose parts resulting from such failures increase the possibility of local flow blockages, which could lead to coolant boiling. Excessive fuel assembly vibration and coolant boiling are therefore potential safety issues, since both conditions could lead to clad failure and fission product release in the primary coolant system. From a design standpoint, the ability to monitor

the in-reactor thermal-hydraulic and mechanical performance of fuel assemblies could lead to improved fuel performance and extended fuel burnup.

In Sect. 2 we discuss previous attempts to determine the ex-core detector response due to in-core perturbations, and in Sect. 3 we present a methodology for calculating detector responses caused by in-core coolant boiling and structural vibrations. Section 4 shows an application of the calculated ex-core detector sensitivities for boiling and vibration to the interpretation of experimental noise data at the Sequoyah-1 PWR. A determination of the feasibility of detecting anomalous fuel assembly vibrations and coolant boiling is presented in Sect. 5, and conclusions and recommendations for future work are contained in Sect. 6.

2. PREVIOUS STUDIES

Previous calculations of the ex-core detector spatial sensitivity to in-core neutron sources and fuel assembly vibrations have been based on either point kernel and discrete ordinates static shielding techniques,[5,9,15-17] or point kinetics.[18] Because the introduction of an external source into a critical reactor results in supercriticality, static techniques model the core as a fixed source of neutrons and as a purely attenuating medium (i.e., $\nu\Sigma_f = 0$). Therefore, source propagation through fission processes was not considered, and the known frequency dependence of the space-dependent reactivity-to-power transfer function was neglected. When static shielding techniques are used to analyze a typical PWR, the ex-core detector spatial sensitivity to in-core neutron sources varies $\sim 10^9$ from the core edge nearest the detector to the core center (i.e., the ex-core detector is sensitive only to neutron sources at the core edge near the detector).[15] Point kinetics techniques assume that the reactor transfer function has no space-dependent effects (i.e., neutron detectors respond with equal magnitude regardless of detector and perturbation locations for equal reactivity inputs), an assumption which has little validity for large, low-enrichment cores in PWRs at frequencies above approximately 0.1 Hz. In short, both point kinetics and static shielding techniques are based on poor or unrealistic assumptions about the kinetic behavior of reactors in the frequency range of most internals vibrations.

Finally, it should be noted that the two-group phenomenological model ("Local" and "Global" noise model) used in boiling water reactors has been applied to calculation of detector responses to control rod vibrations in PWRs.[19-21] This phenomenological model fails to predict the observed behavior of neutron noise when a heterogeneous system is studied (which includes all commercial light water reactors), and the results of this model depend explicitly on the number of neutron energy groups assumed in the calculation.[22-24]

3. GENERAL METHODOLOGY FOR DETERMINING NEUTRON DETECTOR RESPONSE TO IN-CORE PERTURBATIONS

The methodology employed in the present work to determine the ex-core detector spatial sensitivity for in-core perturbations (such as vibrations or boiling) is a combination of the Langevin source conjecture[25] and first-order perturbation approximations. The Langevin source technique assumes that these in-core perturbations can be represented by fluctuating external neutron sources (as opposed to inherent noise sources resulting from statistical fluctuations in neutron reaction processes). The Langevin sources are characterized by the product of a fluctuating macroscopic cross section (due to changes in coolant density for boiling or fuel/moderator displacement for fuel assembly vibrations) with the static (time- or frequency-independent) critical flux. In operator notation, the Langevin source is

$$\delta S(\omega) = \delta\Sigma(\omega)\bar{\phi} \tag{1}$$

where $\delta\Sigma(\omega)$ is a space- and energy-dependent macroscopic cross section fluctuating at frequency ω, and $\bar{\phi}$ is the static, unperturbed, critical flux at the perturbation location. (The Langevin sources for fuel assembly vibrations and boiling are expanded in Sects. 4.2.1 and 4.2.2 respectively.) A fluctuating flux at any detector location resulting from each Langevin source $\delta S(\bar{r}_o, E_o, \bar{\Omega}_o, \omega)$ can be calculated using the forward space-, energy-, and frequency-dependent Boltzmann equation with delayed neutrons, which in standard notation[26] is

$$\bar{\Omega} \cdot \nabla\delta\phi(\bar{r},E,\bar{\Omega},\omega) + \Sigma(\bar{r},E)\ \delta\phi(\bar{r},E,\bar{\Omega},\omega)$$

$$- \int d\bar{\Omega}' \int dE'\ \Sigma_s(\bar{r},E'\bar{\Omega}' \rightarrow E\bar{\Omega})\ \delta\phi(\bar{r},E',\bar{\Omega}',\omega)$$

$$- \left\{ \int d\bar{\Omega}' \int dE'\ \nu\Sigma_f(\bar{r},E',\bar{\Omega}')\ \delta\phi(\bar{r},E',\bar{\Omega}',\omega) \right.$$

$$\left[\frac{(1-\beta)\chi_p(E)}{4\pi} + \sum_j \frac{\chi_j(E)}{4\pi} \frac{\lambda_j \beta_j}{i\omega + \lambda_j} \right] \Bigg\} - \frac{i\omega}{V(E)} \delta\phi(\bar{r},E,\bar{\Omega},\omega)$$

$$= \delta S(\bar{r}_o,E_o,\bar{\Omega}_o,\omega) \tag{2}$$

and in operator notation

$$L\delta\phi = \delta S \quad . \tag{3}$$

For a few detector locations and spatially distributed noise sources it is more convenient to use the equivalent adjoint formulation[26]

$$- \bar{\Omega} \cdot \nabla \phi^+(\bar{r},E,\bar{\Omega},\omega) + \Sigma(\bar{r},E)\, \phi^+(\bar{r},E,\bar{\Omega},\omega)$$

$$- \int d\bar{\Omega}' \int dE' \Sigma_s(\bar{r},E\bar{\Omega}\to E'\bar{\Omega}')\, \phi^+(\bar{r},E',\bar{\Omega}',\omega)$$

$$- \Bigg\{ \int d\bar{\Omega}' \int dE'\, \nu\Sigma_f(\bar{r},E,\bar{\Omega})\, \phi^+(\bar{r},E',\bar{\Omega}',\omega)$$

$$\left[\frac{(1-\beta)\chi_p}{4\pi}(E') + \sum_j \chi_j(E') \frac{\lambda_j \beta_j}{i\omega + \lambda_j} \right] \Bigg\} + \frac{i\omega}{V(E)} \phi^+(\bar{r},E,\bar{\Omega},\omega)$$

$$= -\Sigma_d(\bar{r}_d,E_d,\bar{\Omega}_d) \quad , \tag{4}$$

and in equivalent operator notation is represented by

$$L^+\phi^+ = -\Sigma_d \quad . \tag{5}$$

Assuming a first-order perturbation approximation, the neutron detector response can be represented by

$$R = \langle \Sigma_d \phi \rangle_{V_D} = \langle \phi^+ S \rangle_{V_P} \tag{6}$$

which yields

$$\delta R = \langle \Sigma_d \delta\phi \rangle_{V_D} = \langle \phi^+ \delta S \rangle_{V_P} \tag{7}$$

where δR is the frequency-dependent detector response and $\langle\ \rangle$ indicates phase space integration over the detector volume (V_D) or the perturbation volume (V_P).

The interpretation[26] of the detector adjoint $\phi^+(\bar{r},E,\bar{\Omega},\omega)$ is the importance of a neutron at position $\bar{r}$ with energy E and angular direction $\bar{\Omega}$ in producing a detector response at position $\bar{r}_d$, energy E_d, and angular direction $\bar{\Omega}_d$. An alternate and equivalent interpretation is that the detector adjoint $\phi^+(\bar{r},E,\bar{\Omega},\omega)$ represents the space-, energy-, and frequency-dependent neutron source-to-detector transfer function. It is important to note that the detector adjoint does *not* directly represent the ex-core detector sensitivity for pertubations such as vibration or boiling, since this sensitivity is determined via the convolution of the Langevin source with the detector adjoint (Eq. 7).

It should also be noted that Eqs. 2 and 4 are not defined for the case in which the reactor is critical ($k = 1$) and $\omega = 0$ without feedback, because the insertion of a source for an infinite time period in a critical reactor leads to supercriticality. Equations 2 and 4 are, however, defined for a critical reactor when $\omega \neq 0$. This behavior is due to the decreasing importance of delayed neutrons as ω increases in frequency. This frequency-dependent behavior is similar to that predicted by point kinetics.

The Langevin source formulation (Eq. 1) and the first-order perturbation approximation to the detector response (Eq. 7) imply that the perturbation does not alter the static, critical flux shape, $\bar{\phi}$. We justify these approximations on the basis that only small-amplitude fuel assembly vibrations or coolant density changes (due to boiling) will be considered.

The purpose of the present work is to calculate the ex-core neutron detector response due to stochastic (random) perturbations such as fuel assembly vibrations or boiling. The stochastic nature of neutron noise therefore requires that a statistical description of the signal be employed. The statistical properties of a perturbation are accounted for by an expectation operator $E\{\ \}$.[27] The statistical description of the detector response is therefore characterized by a statistical description of the perturbation. For a single perturbation

$$E\left\{\delta R^2\right\} = E\left\{\langle \phi^+ \delta S\rangle_{V_P}^2\right\} \tag{8}$$

where $E\{\delta R^2\}$ is the mean square of the detector response and it is assumed that the mean response $E\{\delta R\} = 0$.

When multiple perturbations are considered, statistical descriptors of the individual perturbations, as well as their statistical relationship with each other (joint probability density), must be included.

$$E\left\{\delta R^2\right\} = E\left\{\sum_k \sum_\ell \langle \phi^+ \delta S\rangle_{V_{P_k}} \langle \phi^+ \delta S\rangle_{V_{P_\ell}}\right\} . \tag{9}$$

In order to determine the detector response to multiple perturbations, it is therefore necessary to have an *a priori* knowledge of the statistical relationships between the perturbations. Usually, the detector response is determined for statistically correlated sources (as might result from multiple perturbations caused by a common driving force) so that Eq. 9 becomes

$$E\left\{\delta R^2\right\}_{\text{corr.}} = E\left\{\left(\sum_k \langle \phi^+ \delta S\rangle_{V_{P_k}}\right)^2\right\} \tag{10}$$

or statistically uncorrelated perturbations (as might result from independent driving forces) yielding

$$E\left\{\delta R^2\right\}_{\text{uncorr.}} = \sum_k E\left\{\left(\langle \phi^+ \delta S\rangle_{V_{P_k}}\right)^2\right\} \tag{11}$$

Eq. 11 shows that the mean square of the detector response due to multiple uncorrelated perturbations is simply the sum of the mean squares for each of the individual perturbations. Expanding Eq. 10, the mean square detector response for correlated perturbations is

$$E\left\{\delta R^2\right\}_{\text{corr.}} = E\left\{\langle\phi^+\delta S\rangle_{V_{P_1}}{}^2\right\} + E\left\{\langle\phi^+\delta S\rangle_{V_{P_2}}{}^2\right\} + \ldots$$

$$+ 2E\left\{\langle\phi^+\delta S\rangle_{V_{P_1}} \langle\phi^+\delta S\rangle_{V_{P_2}}\right\} + 2E\left\{\langle\phi^+\delta S\rangle_{V_{P_1}} \langle\phi^+\delta S\rangle_{V_{P_3}}\right\} + \ldots, \qquad (12)$$

which is the sum of the individual mean squares and the cross correlations between the perturbations. It can be seen from the above that the calculated detector response to multiple perturbations depends directly on the assumed importance of the cross correlation between individual sources.

The steps for determining the detector response due to perturbations were thus: (a) Solve Eq. 4 for each detector location; (b) calculate the Langevin source for each type of perturbation via Eq. 1; (c) compute the detector response by convolving the Langevin source with the detector and integrating over neutron energy and source volume as indicated in Eq. 7; and (d) apply the expectation operator under the assumptions of spatially correlated or uncorrelated perturbations to yield statistical descriptors of the resulting neutron detector responses.

4. CALCULATION OF THE EX-CORE DETECTOR RESPONSE DUE TO COOLANT BOILING AND VIBRATIONS

4.1 DETECTOR ADJOINT CALCULATIONS

4.1.1 One-Dimensional Calculations

Solutions to the multigroup, one-dimensional slab, discrete ordinates form (as shown in Appendix A) of the detector adjoint equations (Eq. 4) were obtained using a modified version of the TASK[28] computer code. The TASK code was utilized to perform S_4 angular quadrature, detector adjoint calculations for the one-dimensional slab geometry shown in Fig. 1. The calculations were performed using a P_3, 3-neutron energy group cross section set and 6 delayed-neutron groups collapsed from a 27-group library based on the ENDF-B/V cross section library. The methods used to generate this cross section set are described in Appendix C. The ex-core detector was assumed to be sensitive only to neutrons in the thermal energy group. All calculations were performed at ω = 3 Hz, since this has been shown by several studies[11,29,30] to be the approximate natural (first mode) frequency for PWR fuel assembly vibrations. Static, eigenvalue calculations were performed using the ANISN[31] discrete ordinates code with P_3 scattering and S_4 angular quadrature to determine the static flux $\bar{\phi}$. The reactor was made exactly critical (k = 1) using ANISN by adjusting the transverse leakage (DB^2 losses) and an equivalent burnable poison concentration (soluble poison and burnable posion rods) of ~2100 ppm boron. All calculations were performed by requiring relative errors of $<10^{-4}$ for both the eigenvalue and fluxes between iterations.

The following cases were studied:

(a) k = 1, equivalent boron concentration 2100 ppm
(b) k = 0.995 (altered transverse leakage)
(c) k = 1, equivalent boron concentration 2150 ppm
(d) k = 1, equivalent boron concentration 2100 ppm, pressure vessel and concrete biological shield included in the model.

ORNL-DWG 84-8846

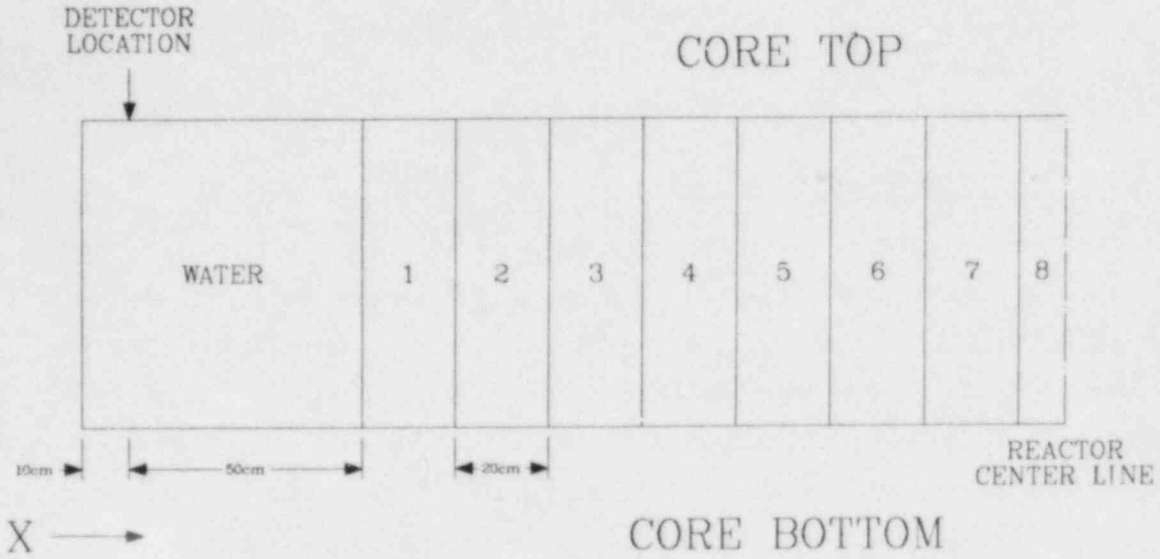

FUEL ELEMENT	U-235 ENRICHMENT (W%)
1	3.18
2	3.18
3	2.0
4	2.55
5	2.0
6	2.55
7	2.0
8	2.55

FJS011 81J

Fig. 1. One-dimensional slab geometry for transport calculations of cases (a), k = 1, equivalent boron concentration 2100 ppm; (b), k = 0.995 (altered transverse leakage); and (c), k = 1, equivalent boron concentration 2150 ppm.

In addition to these cases, a one-dimensional diffusion solution to the detector adjoint equation was obtained using the JPRKINETICS[32] code in case (a).

4.1.2 Results of One-Dimensional Detector Adjoint Calculations

Figure 2 shows the detector adjoint magnitudes for thermal energy group neutrons for cases (a) and (b) above. The magnitude of the detector adjoint in the core is seen to be sensitive to the assumed criticality state (k) of the reactor. Unlike the results of static shielding

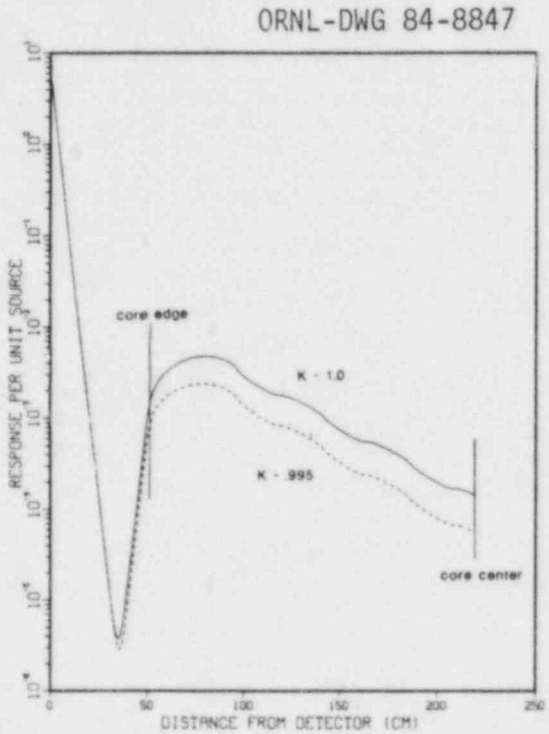

Fig. 2. Thermal group detector adjoint magnitudes at 3 Hz for k = 1.0 [case (a)] and k = .995 [case (b)].

calculations,[15,16] the detector adjoints shown in Fig. 2 decrease by less than one order of magnitude from the core edge nearest the detector to the core centerline since the previous calculations did not account for source propagation through fission processes. The space-dependent nature of the detector adjoint inside the core indicates that, as expected, point kinetic theory is also a poor approximation of large PWR cores at a frequency of 3 Hz.

The sensitivity of the calculated detector adjoints to small changes in boron concentration was studied by increasing the equivalent poison concentration to 2150 ppm and then readjusting the transverse leakage so that the core was again exactly critical [case (c)]. The results were practically indistinguishable from case (a), indicating that the detector adjoints are not sensitive to small changes in boron concentration.

To study the effect of the steel pressure vessel and concrete biological shield on the detector response, the core was modeled as shown in Fig. 1, with the outer 30 cm of water replaced by 10 cm of concrete behind the detector and 20 cm of steel between the detector and the core. The air gap between the pressure vessel and the biological shield occurring in PWRs was treated as a vacuum, and the detector was located at the biological shield/pressure vessel interface. Figure 3 compares the thermal-group detector adjoints computed for the two geometric modelings, cases (a) and (d). For these cases, the relative attenuation of the detector sensitivity across the core does not change appreciably; however, the difference in the absolute magnitude of the adjoints is approximately one order of magnitude. For each case the magnitudes of the thermal, epithermal, and fast groups were approximately equal inside the core but varied significantly outside the core (as will be shown in the next section). These results indicate that the inclusion of different ex-core materials will probably not markedly affect the *relative* sensitivity with which neutron sources can be detected at different in-core locations, but the magnitudes of the detector responses predicted by these calculations will be heavily influenced.

One-dimensional detector adjoints were calculated using both TASK and JPRKINETICS for case (a). The VENTURE[33] code was utilized to adjust the critical boron concentration for the diffusion calculations, resulting in an equivalent boron concentration of 2160 ppm. The results of these calculations are compared in Fig. 4 and show that diffusion theory is adequate for the model assumed. As expected, it was found that the calculated detector adjoints were sensitive to the diffusion coefficients of the ex-core materials.

4.1.3 Two-Dimensional Diffusion Calculations of the Detector Adjoint

Two-dimensional diffusion calculations of the ex-core detector adjoint were performed for an X-Y (radial) plane model of the Sequoyah-1 core shown in Fig. 5 using the JPRKINETICS code. Three neutron energy

ORNL-DWG 84-8848

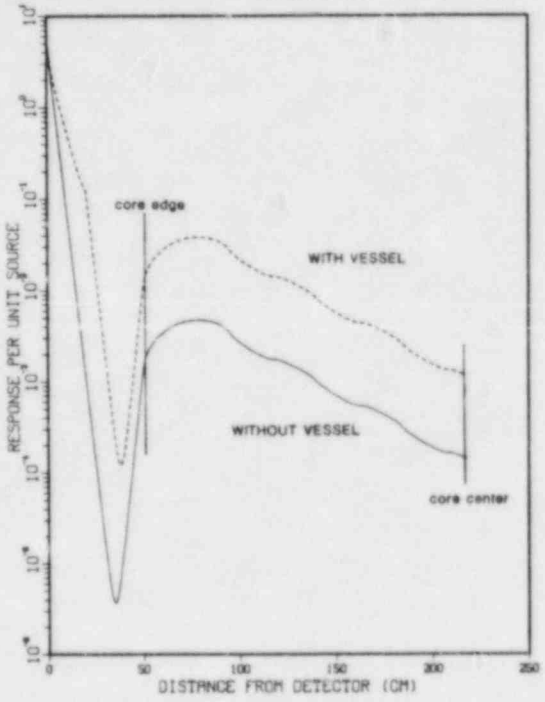

Fig. 3. Thermal group detector adjoint magnitudes at 3 Hz for slab geometry with case (a) and without case (d) ex-core structural materials

ORNL-DWG 84-8849

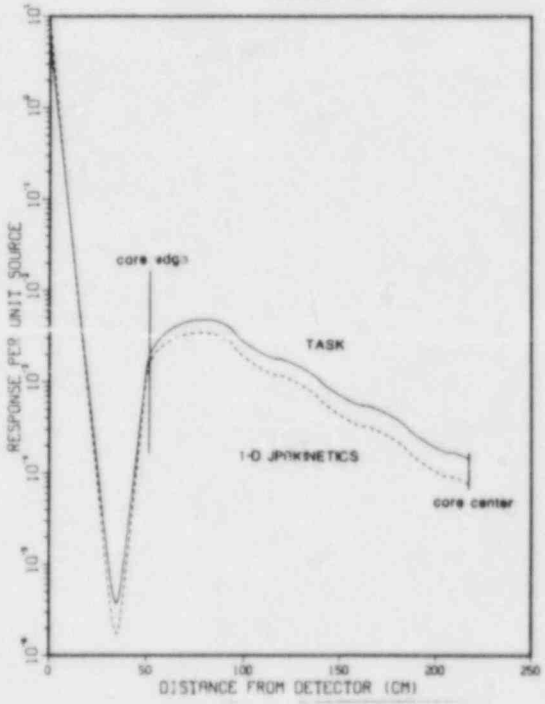

Fig. 4. Comparison of the thermal group detector adjoint magnitudes at 3 Hz calculated with transport theory (TASK) and diffusion theory (JPRKINETICS) for case (a).

groups and six delayed-neutron groups were generated as described in Appendix C for the following conditions:

1. Beginning of Cycle (BOC), no burnable poison rods (NBPR), no xenon, 1950 ppm soluble boron

2. BOC, NBPR, equilibrium xenon, 1580 ppm soluble boron

3. End of Cycle (EOC), NBPR, equilibrium xenon, 120 ppm soluble boron

4. BOC, burnable poison rods (BPR), equilibrium xenon, 780 ppm soluble boron

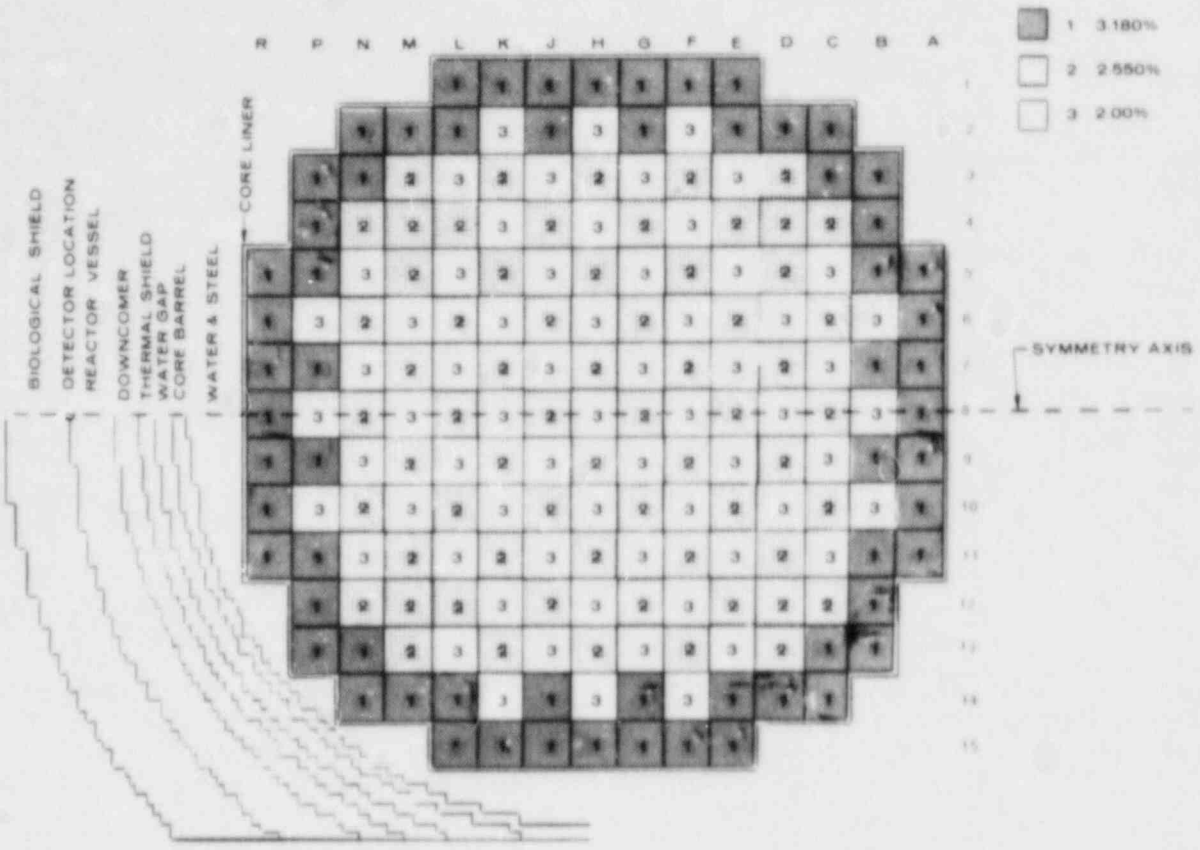

Fig. 5. X-Y (radial) plane model of the Sequoyah-1 PWR core for two-dimensional diffusion calculations.

5. EOC, BPR, equilibrium xenon, 100 ppm soluble boron

6. BOC, BPR, no fission ($\nu\Sigma_f = 0$), 780 ppm soluble boron

For these cases, isotopic depletion and buildup were considered over approximately one fuel cycle, including changes in delayed-neutron parameters. Boron concentrations were adjusted to achieve a critical core using the VENTURE static diffusion theory code. For both VENTURE and JPRKINETICS calculations, point convergence criteria and point balances were held to $<10^{-4}$ relative error.

4.1.4 Results of Two-Dimensional Adjoint Calculations

The detector adjoints for the no xenon and equilibrium xenon cases (cases 1 and 2) at the BOC with NBPR are presented in Figs. 6 and 7 respectively. A comparison of these two cases shows that xenon poisons strongly affect the detector spatial sensitivity for neutron sources due to its non-uniform spatial concentration. Comparison of the NBPR and BPR results for both the BOC (cases 2 and 4) and the EOC (cases 3 and 5) in Figs. 7 through 10, respectively, shows that burnable poison rods, boron concentration, and isotopic changes due to fuel burnup have relatively little effect on the shape and magnitude of the calculated detector adjoints. An important outcome of these calculations is that the ex-core detector is nearly equally sensitive to fast, epithermal, and thermal neutron sources inside the core in contrast to results of previous shielding calculations.[15-17]

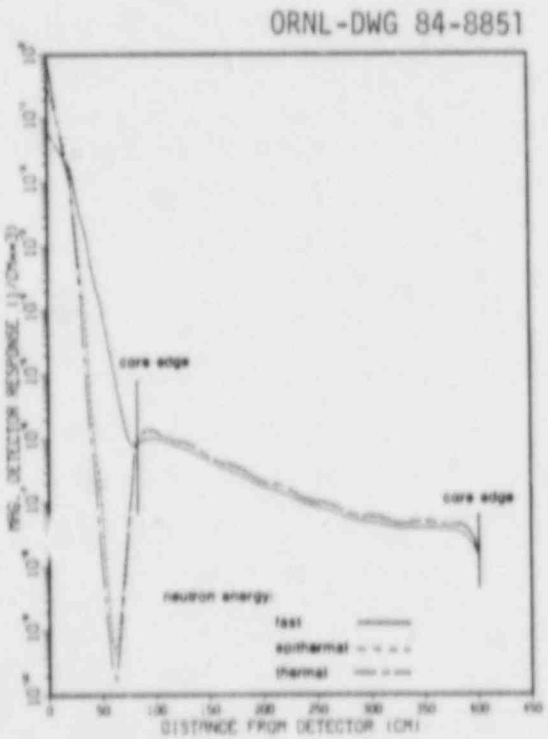

Fig. 6. Detector adjoint magnitudes at 3 Hz along the symmetry axis: beginning of cycle, no burnable poison rods, and no xenon (case 1).

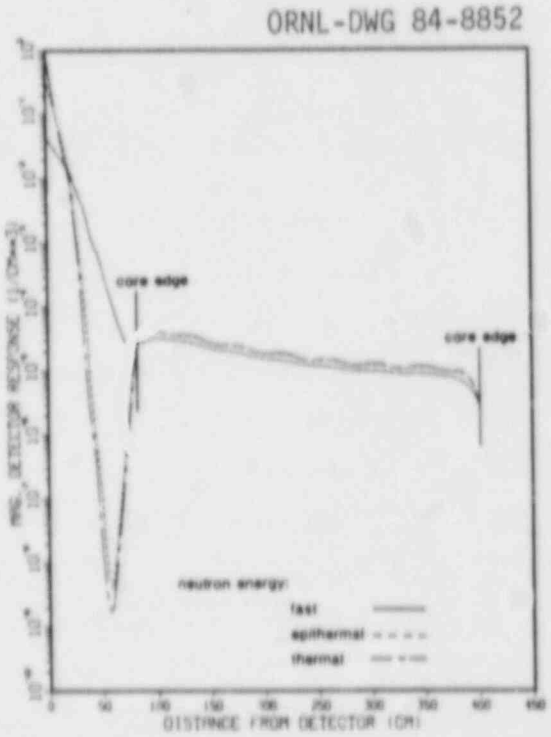

Fig. 7. Detector adjoint magnitudes at 3 Hz along the symmetry axis: beginning of cycle, no burnable poison rods, and equilibrium xenon (case 2).

ORNL-DWG 84-8853

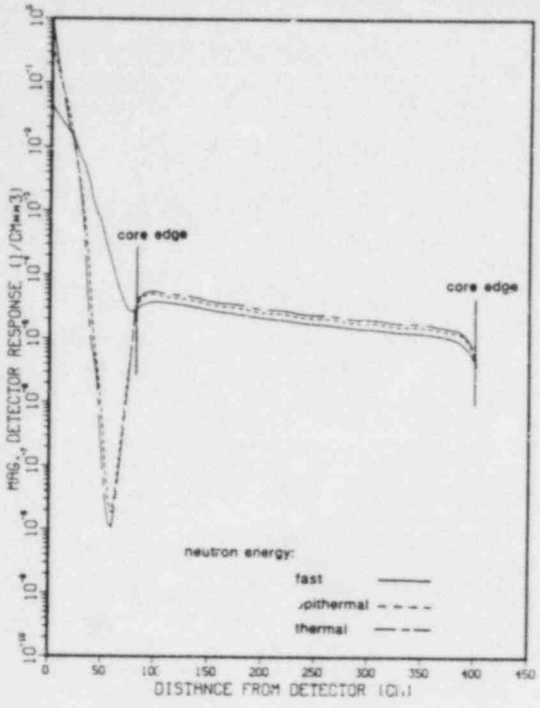

Fig. 8. Detector adjoint magnitudes at 3 Hz along the symmetry axis: end of cycle, no burnable poison rods, and equilibrium xenon (case 3).

ORNL-DWG 84-8854

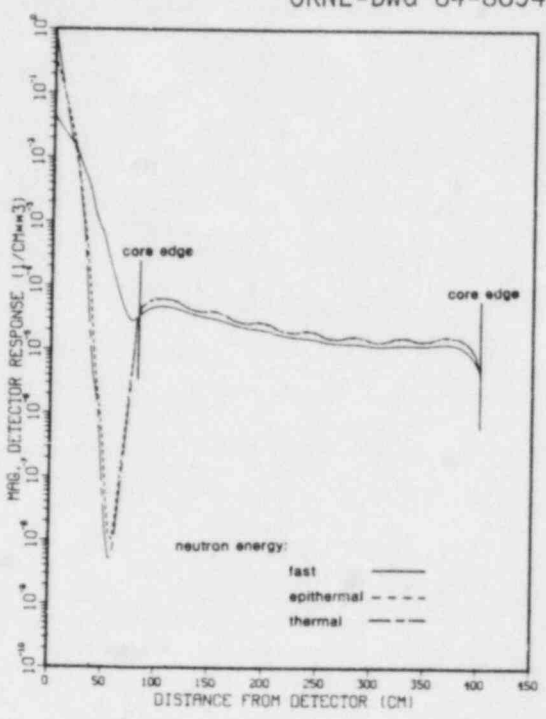

Fig. 9. Detector adjoint magnitudes at 3 Hz along the symmetry axis: beginning of cycle, burnable poison rods, and equilibrium xenon (case 4).

A detector adjoint calculation was performed in which no fission was assumed ($\nu\Sigma_f = 0$, case 6) as in refs. 6, 9, and 15-17. When no fission is assumed, the core becomes an attenuating (shielding) material so that only an exponential decrease in the detector spatial sensitivity occurs (Fig. 11) and the detector sensitivity to fast neutrons dominates in all regions. The fast detector adjoint was normalized to a value of 1.0 at the core edge nearest the detector, and the results are presented in Fig. 12. The normalized detector adjoint in which no fission was assumed shows good agreement with the ex-core detector spatial "weighting function" calculated by Crump and Lee.[15] This comparison indicates that the works in refs. 6, 9, and 15-17 do not account for neutron propagation

ORNL-DWG 84-8855

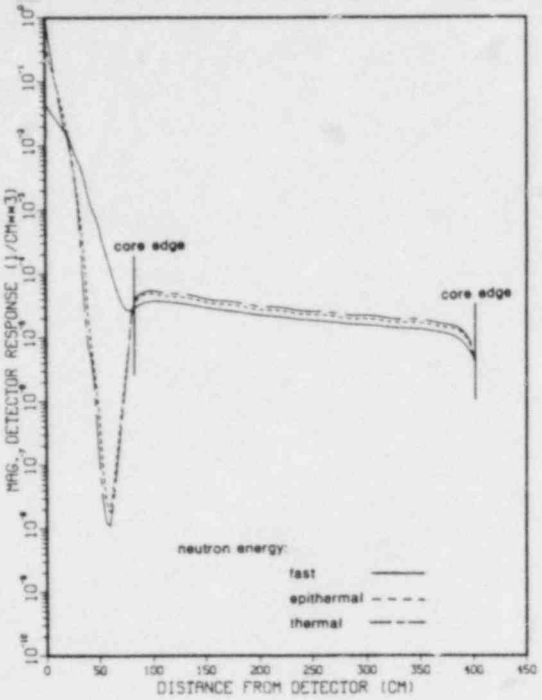

Fig. 10. Detector adjoint magnitudes at 3 Hz along the symmetry axis: end of cycle, burnable poison rods, and equilibrium xenon (case 5).

ORNL-DWG 84-8856

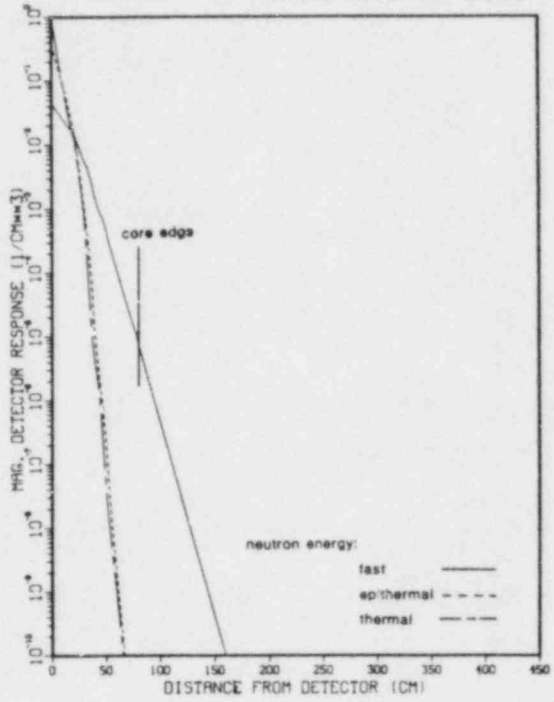

Fig. 11. Detector adjoint magnitudes at 3 Hz along the symmetry axis: beginning of cycle, burnable poison rods, equilibrium xenon, and no fission ($\nu\Sigma_f = 0$) (case 6).

through fission processes in the core and therefore underpredict the ex-core detector sensitivity to in-core neutron sources by as much as 20 orders of magnitude.

Phase shifts between the source and detector locations presented in Figs. 13-17 for cases 1 through 5, respectively, are large (as much as 20°) at 3 Hz for sources inside the core. For the no-fission case (6), phase shifts are always <5° as shown in Fig. 18. The imaginary part of the detector adjoint (and therefore the phase shift) is determined by the $i\omega/V(E)$ and delayed neutron terms of Eq. 4. Since only the $i\omega/V$ term is present in the no-fission case, we conclude that this term is small at 3 Hz and that the phase shifts are primarily determined by the delayed

ORNL-DWG 84-8857

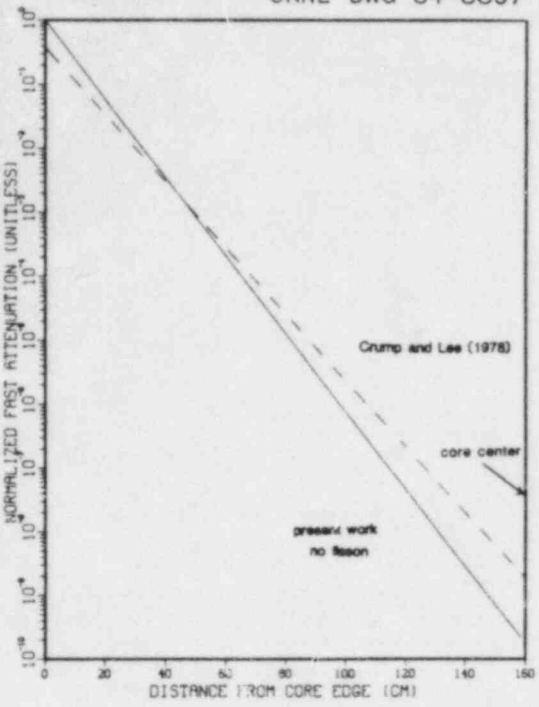

Fig. 12. Comparison of the normalized fast detector adjoint magnitude with no fission ($\nu\Sigma_f = 0$, case 6) with the spatial weighting function of ref. 15.

ORNL-DWG 84-8858

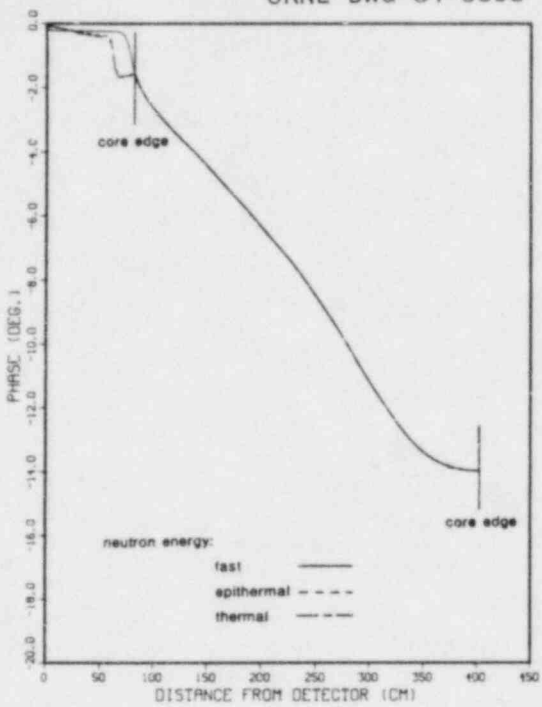

Fig. 13. Detector adjoint phase at 3 Hz along the symmetry axis for case 1 (beginning of cycle, no burnable poison rods, no xenon).

neutrons. These large phase shifts also indicate that static (time- or frequency-independent) techniques are not adequate in analyzing the ex-core spatial sensitivity for neutron sources since no imaginary part of the detector response (and therefore phase shift) is accounted for.

Changes in the calculated phase shifts are small (<5°) from BOC to EOC for both the BPR and NBPR cases. These changes are not uniform across the core because the different isotopic buildup and depletion rates occurring with burnup also affect the spatial distribution of delayed-neutron parameters.

4.2 DETECTOR RESPONSE TO FUEL ASSEMBLY VIBRATIONS AND COOLANT BOILING

In order to determine the detector response to a specific in-core perturbation such as fuel assembly vibration or coolant boiling, the

ORNL-DWG 84-8859

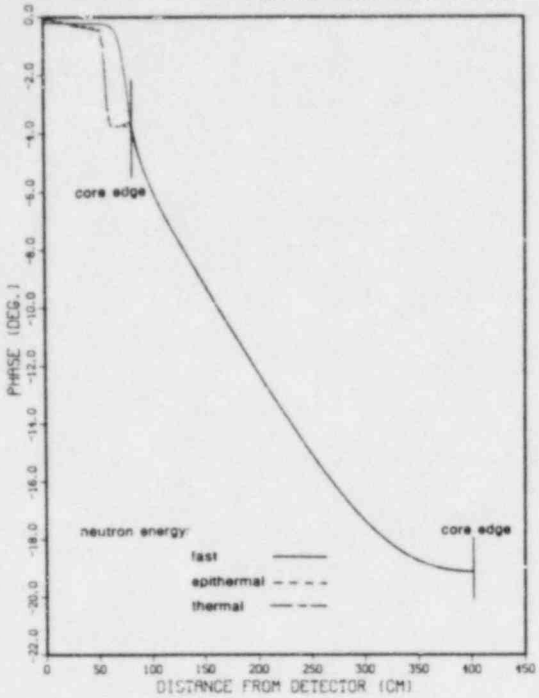

Fig. 14. Detector adjoint phase at 3 Hz along the symmetry axis for case 2 (beginning of cycle, no burnable poison rods).

ORNL-DWG 84-8860

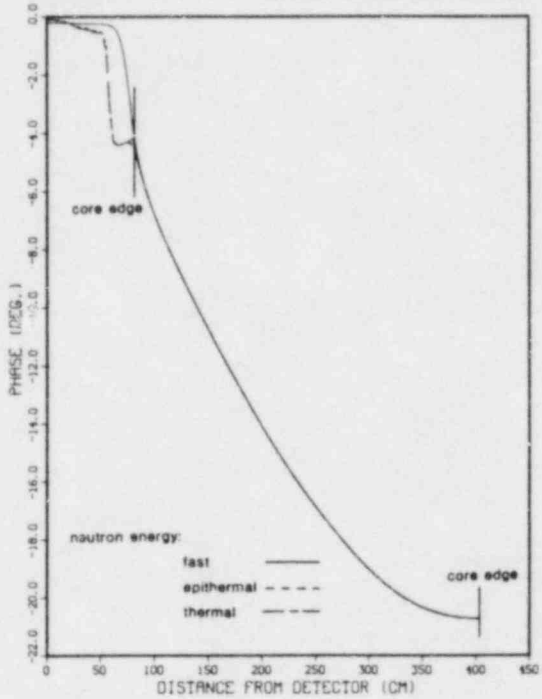

Fig. 15. Detector adjoint phase at 3 Hz along the symmetry axis for case 3 (end of cycle, no burnable poison rods).

ORNL-DWG 84-8861

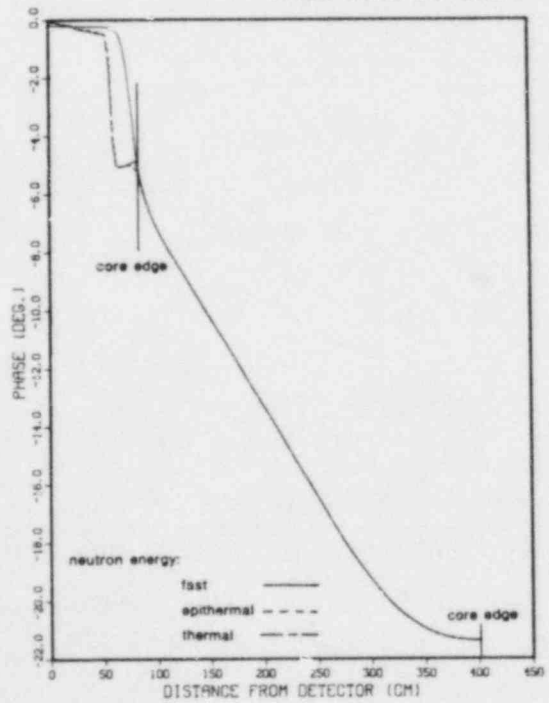

Fig. 16. Detector adjoint phase at 3 Hz along the symmetry axis for case 4 (beginning of cycle, burnable poison rods).

ORNL-DWG 84-8862

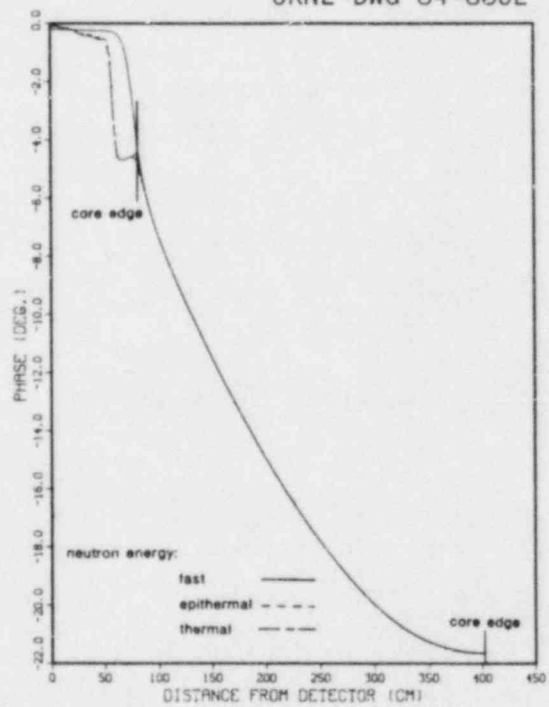

Fig. 17. Detector adjoint phase at 3 Hz along the symmetry axis for case 5 (end of cycle, burnable poison rods).

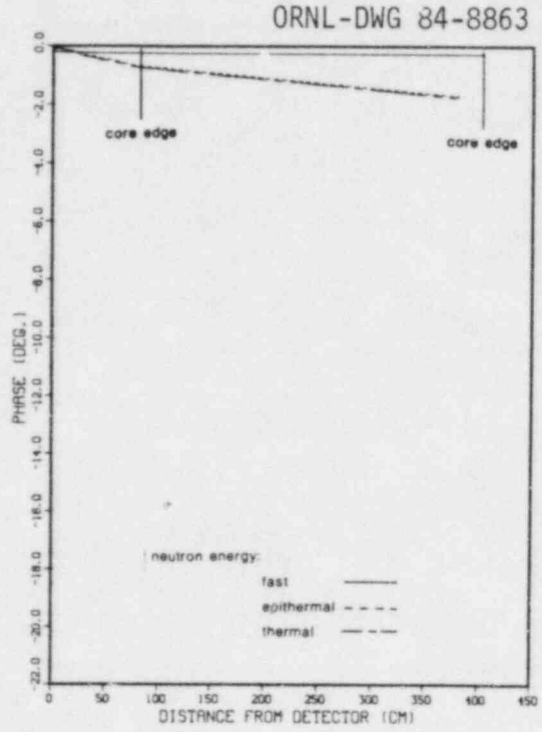

Fig. 18. Detector adjoint phase at 3 Hz along the symmetry axis for case 6 (beginning of cycle, burnable poison rods, $\nu\Sigma_f = 0$),

perturbation is modeled as a fluctuating neutron source (Langevin source) and combined with the detector adjoints presented in the previous section. Since the Langevin source varies with each type of perturbation considered, detector response and therefore detector spatial sensitivity for each perturbation also varies.

4.2.1 Langevin Source for Fuel Assembly Vibrations

The Langevin source for fuel assembly vibrations is derived by assuming that the fuel assembly moves and displaces moderator on one side of the assembly while moderator replaces the fuel on the other side of the assembly, as shown in Fig. 19. Assuming that the change in composition occurs on each side of the assembly, a first-order perturbation approximation to the detector response is

$$
\begin{aligned}
\delta R^{G_d}(r_d,\omega) = -\sum_g \Bigg[& \left(\Sigma_{a_w}^{g}(r_1) - \Sigma_{a_c}^{g}(r_1)\right) \phi^{g}(r_1)\, \phi^{+g}(r_1,\omega) dV_1 \\
& + \left(\Sigma_{a_c}^{g}(r_2) - \Sigma_{a_w}^{g}(r_2)\right) \phi^{g}(r_2)\, \phi^{+g}(r_2,\omega) dV_2 \Bigg] \\
& + \sum_g \Bigg\{ \phi^{+g}(r_1,\omega) \sum_{\substack{g' \\ g' \neq g}} \Bigg[\left(\Sigma_{s_w}^{g' \to g}(r_1) - \Sigma_{s_c}^{g' \to g}(r_1)\right) \phi^{g'}(r_1) \\
& - \left(\Sigma_{s_w}^{g \to g'}(r_1) - \Sigma_{s_c}^{g \to g'}(r_1)\right) \phi^{g}(r_1) \Bigg] dV_1 \\
& + \phi^{+g}(r_2,\omega) \sum_{\substack{g' \\ g' \neq g}} \left[\left(\Sigma_{s_c}^{g' \to g}(r_2) - \Sigma_{s_w}^{g' \to g}(r_2)\right) \phi^{g'}(r_2) - \left(\Sigma_{s_c}^{g \to g'}(r_2) - \Sigma_{s_w}^{g \to g'}(r_2)\right) \phi^{g}(r_2) \right] dV_2 \Bigg\} \\
& + \sum_g \Bigg\{ \phi^{+g}(r_1,\omega) \sum_{\substack{g' \\ g' \neq g}} \Bigg[\nabla \left(DD_w^{g' \to g}(r_1) - DD_c^{g' \to g}(r_1)\right) \nabla \phi^{g'}(r_1) \\
& - \nabla \left(DD_w^{g \to g'}(r_1) - DD_c^{g \to g'}(r_1)\right) \nabla \phi^{g}(r_1) \Bigg] dV_1 \\
& + \phi^{+g}(r_2,\omega) \sum_{\substack{g' \\ g' \neq g}} \Bigg[\nabla \left(DD_c^{g' \to g}(r_2) - DD_w^{g' \to g}(r_2)\right) \nabla \phi^{g'}(r_2) \\
& - \nabla \left(DD_c^{g \to g'}(r_2) - DD_w^{g \to g'}(r_2)\right) \nabla \phi^{g}(r_2) \Bigg] dV_2 \Bigg\} \\
& + \sum_g \Bigg\{ \phi^{+g}(r_1,\omega) \sum_{g'} \left[\chi^{g' \to g} \nu\Sigma_f^{g'}(r_1) \phi^{g'}(r_1) \right] dV_1 \\
& - \phi^{+g}(r_2,\omega) \sum_{g'} \left[\chi^{g' \to g} \nu\Sigma_f^{g'}(r_2)\, \phi^{g'}(r_2) \right] dV_2 \Bigg\} \qquad (13)
\end{aligned}
$$

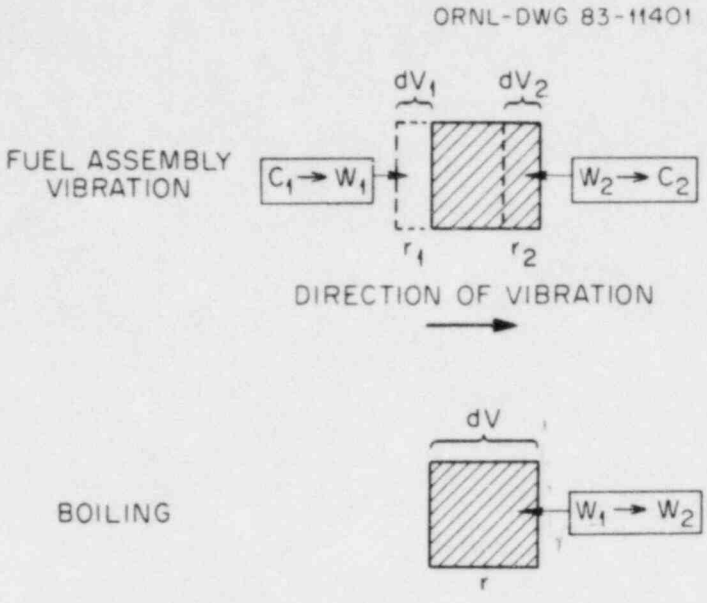

Fig. 19. Langevin source formulation for a vibrating fuel assembly and for coolant boiling.

If a fuel assembly is assumed to be incompressible (i.e., the fuel assembly does not expand or contract with displacement), then $dV_1 = dV_2 = dV$. All calculations presented in this work were performed using Eq. 13 with $dV_1 = dV_2 = dV$. Note that the various cross sections on each side of a fuel assembly are not necessarily the same because of differences in the neutron spectra used to collapse the fine-group to broad-group cross section sets.

Each of the terms in Eq. 13 represents a contribution to the detector response from a specific neutronic process. Previous calculations[34] have shown that none of the terms for fuel assembly vibrations in this equation can be ignored in a critical PWR.

In order to gain a further understanding of the relationship between fuel assembly vibrations and neutron detector response, Eq. 13 can be simplified by assuming that the material properties w and c are the same at r_1 and r_2, and $dV = dV_1$ (for x-y geometry). Equation 13 can then be written in operator notation for fuel assembly vibrations

$$\delta R^{G_d}(r_d,\omega) = \sum_g \left\{ \phi^{+g}(r_1,\omega)\left[\sum_{g'}\left(\Sigma_w^{g',g} - \Sigma_c^{g',g}\right)\phi^{g'}(r_1)\right] \right.$$

$$\left. - \phi^{+g}(r_2,\omega)\left[\sum_{g'}\left(\Sigma_w^{g',g} - \Sigma_c^{g',g}\right)\phi^{g'}(r_2)dV_2\right]\right\} dV \qquad (14)$$

where $\Sigma_w^{g',g}$ and $\Sigma_c^{g',g}$ contain cross section and ∇ operator terms which lead to a gain or loss of neutrons in group g. Equation 14 shows that the detector response is due to two Langevin sources, one on either side of the fuel assembly, that are 180° out of phase with each other. Furthermore, Eq. 14 shows that even though there might be no net reactivity insertion due to fuel assembly vibration, that is,

$$\left(\Sigma_w^{g',g'} - \Sigma_c^{g,g'}\right)\left(\phi^{g'}(r_1) - \phi^{g'}(r_2)\right) = 0 \quad ,$$

a detector response is still possible due to the fuel assembly moving through a gradient in the detector spatial sensitivity, i.e.,

$$\phi^{+g}(r_1,\omega) - \phi^{+g}(r_2,\omega) \neq 0 \quad .$$

It can be seen that no detector response will occur when the fuel assembly moves through symmetric flux and symmetric adjoint gradients, and possesses identical material properties on each side of the assembly. It can also be seen from Eq. 14 that lateral (side to side) and frontal (toward and away) vibrations in reference to the detector location will yield detector responses of different magnitudes if there are differences in flux and adjoint gradients in the frontal and lateral directions.

4.2.2 Langevin Source for Coolant Boiling

The Langevin source for boiling is handled in a manner similar to the fuel assembly vibrations. It is assumed that a change in the

moderator density occurs from w_1 to w_2 in volume dV, and therefore the detector response is approximated by

$$\delta R^{G_d}(r_d,\omega) = -\sum_g \left(\Sigma^g_{a_{w_1}}(r) - \Sigma^g_{a_{w_2}}(r)\right)\phi^{+g}(r,\omega)dV$$

$$+\sum_g \phi^{+g}(r,\omega)\sum_{g'}\left[\left(\Sigma^{g'\to g}_{s_{w_1}} - \Sigma^{g'\to g}_{s_{w_2}}\right)\phi^{g'}(r) - \left(\Sigma^{g\to g'}_{s_{w_1}} - \Sigma^{g\to g'}_{s_{w_2}}\right)\phi^{g}(r)\right]dV$$

$$+\sum_g \phi^{+g}(r,\omega)\sum_{\substack{g'\\ g'\neq g}}\left[\nabla\left(DD^{g'\to g}_{w_1} - DD^{g'\to g}_{w_2}\right)\nabla\phi^{g'}(r) - \nabla\left(DD^{g'\to g}_{w_1} - DD^{g'\to g}_{w_2}\right)\nabla\phi^{g}(r)\right]dV. \quad (15)$$

The detector response for moderator boiling differs from the response to fuel assembly vibrations in that there are no perturbations in fissile concentration ($\delta\nu\Sigma_f = 0$). In operator notation the detector response can be written as

$$\delta R^{G_d}(r_d,\omega) = \sum_g \phi^{+g}(r,\omega)\sum_{g'}\left(\Sigma^{g',g}_{w_1} - \Sigma^{g',g}_{w_2}\right)\phi^{g'}(r)dV \quad (16)$$

which does not depend on perturbations moving through gradients in the flux or adjoint. Therefore, unlike fuel assembly vibrations, moderator boiling inside the reactor system will always produce a detector response.

4.2.3 Results of Fuel Assembly Vibration Calculations

The ex-core detector response to fuel assembly vibrations was calculated for cases 1-6 of Sect. 4.2.1 assuming driving forces that were either spatially correlated (as might result from vibrations induced by core barrel motion) or uncorrelated (as might result from flow-induced vibrations). All fuel assemblies were assumed to vibrate with equal amplitude and with random direction. The total detector response resulting from the superposition of each fuel assembly vibration was calculated

and normalized to the steady state (mean) detector response. The normalized root mean square detector response was determined using Eqs. 10 and 11 for correlated and uncorrelated driving forces respectively. The results were then normalized to the assumed vibrational amplitude to yield a scale factor in NRMS/cm (Table 1).

These calculations yielded the following results:

- Spatially correlated vibrations yield total scale factors about one order of magnitude larger than when spatially uncorrelated vibrations are assumed.

- The detector response for fuel assembly vibrations increases with burnup even if the amplitude of vibration remains constant. Fuel assembly vibrations at the EOC produce about twice the ex-core detector response compared to the BOC for both BPR and NBPR cores.

- NBPR cores yield noise increases 10-20% larger than BPR cores over the first fuel cycle.

The ex-core detector response to the vibration of each individual fuel assembly was calculated for cases 1 through 6, and the fractional contribution to the total detector response was determined under the assumptions of spatially correlated and uncorrelated equal amplitude vibrations. The results for vibrations along the symmetry axis are presented in Figs. 20-25 for cases 1 through 6 respectively. We made the following observations:

- For the fission cases (cases 1 through 5) no single fuel assembly contributes more than ~3.5% to the total detector response when all fuel assemblies vibrate with equal amplitude.

- Individual correlated vibrations contribute more than uncorrelated vibrations to the total detector response for all fuel assembly

Table 1. Calculated ex-core detector scale factors for fuel assembly vibrations in a Westinghouse PWR

	Total scale factors[a]					
	Beginning of cycle		End of cycle		% increase	
	BPR[b]	NBPR[c]	BPR	NBPR	BPR	NBPR
correlated	6.0	5.1	9.5	9.0	58	77
uncorrelated	0.7	0.6	1.1	1.0	58	67

[a]Units are NRMS per cm of fuel assembly vibration normalized to the mean detector response. All fuel assemblies are assumed to vibrate with the same amplitude.

[b]Burnable poison rods.

[c]No Burnable poison rods.

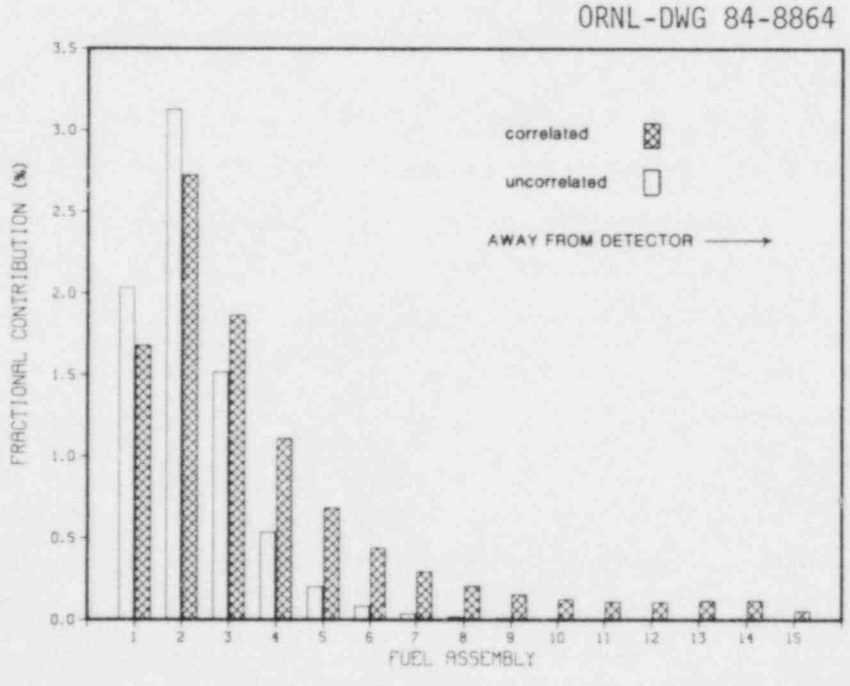

Fig. 20. Fractional contribution to the total ex-core detector response from fuel assembly vibrations along the symmetry axis for case 1 (beginning of cycle, no burnable poison rods, no xenon).

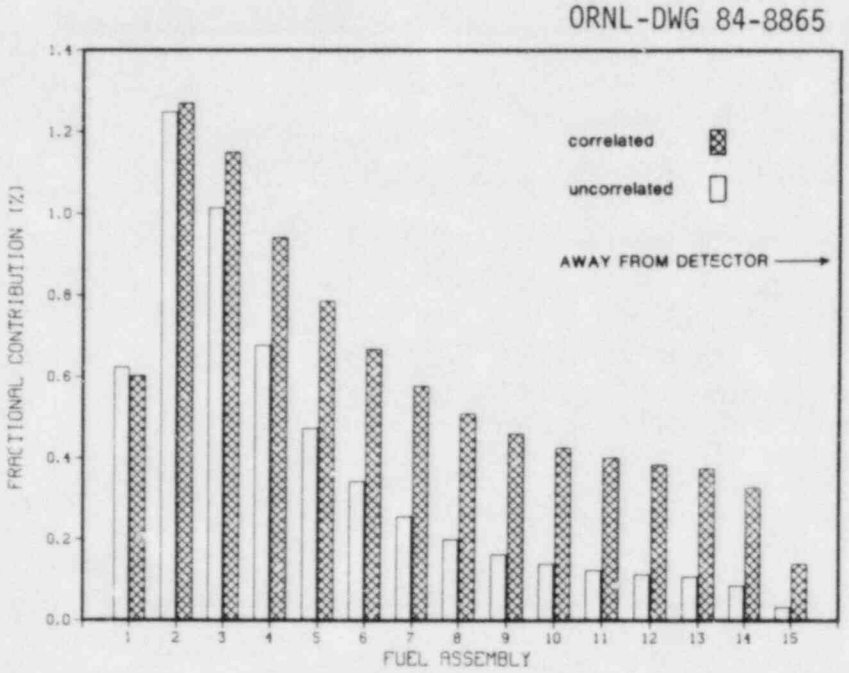

Fig. 21. Fractional contribution to the total ex-core detector response from fuel assembly vibrations along the symmetry axis for case 2 (beginning of cycle, no burnable poison rods).

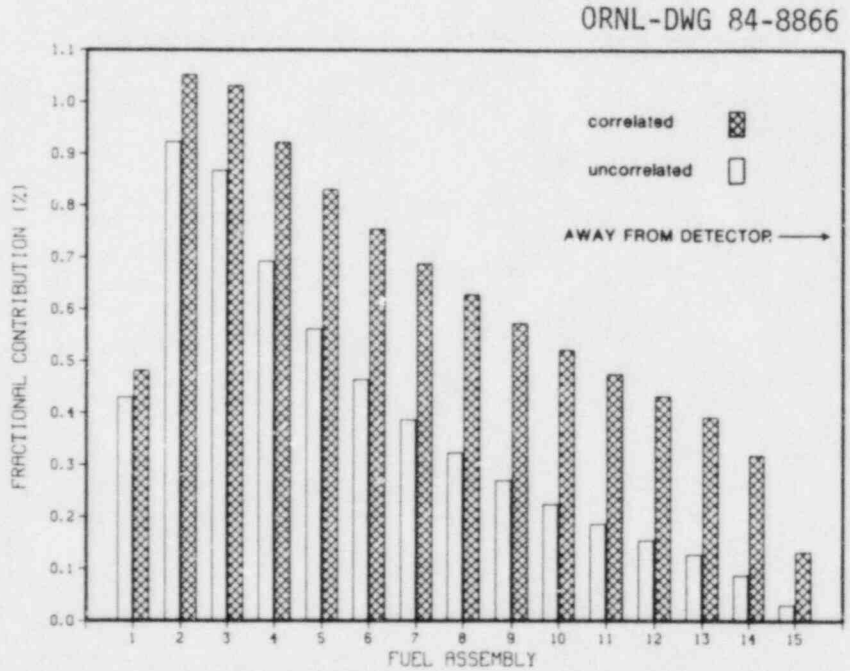

Fig. 22. Fractional contribution to the total ex-core detector response from fuel assembly vibrations along the symmetry axis for case 3 (end of cycle, no burnable poison rods).

ORNL-DWG 84-8867

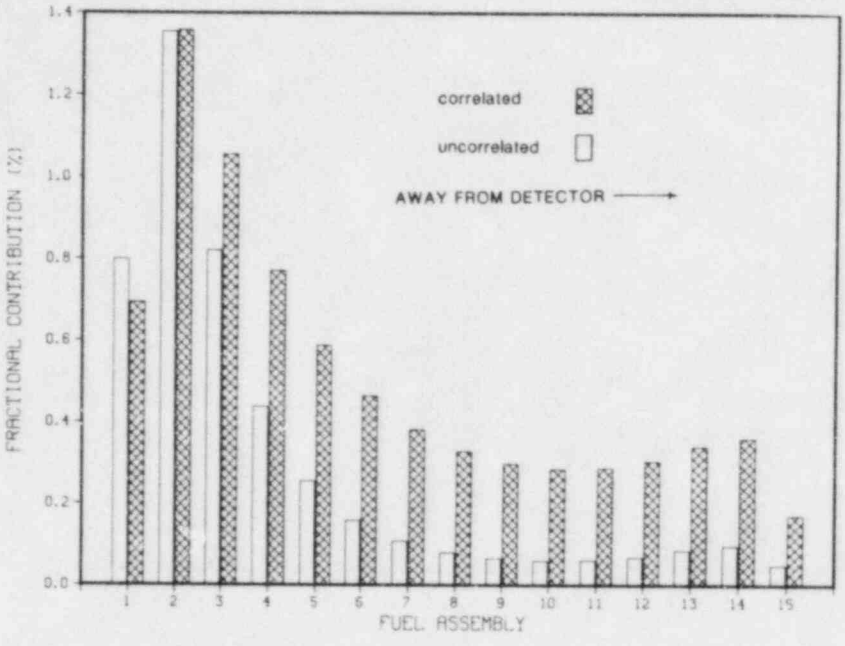

Fig. 23. Fractional contribution to the total ex-core detector response from fuel assembly vibrations along the symmetry axis for case 4 (beginning of cycle, burnable poison rods).

ORNL-DWG 84-8868

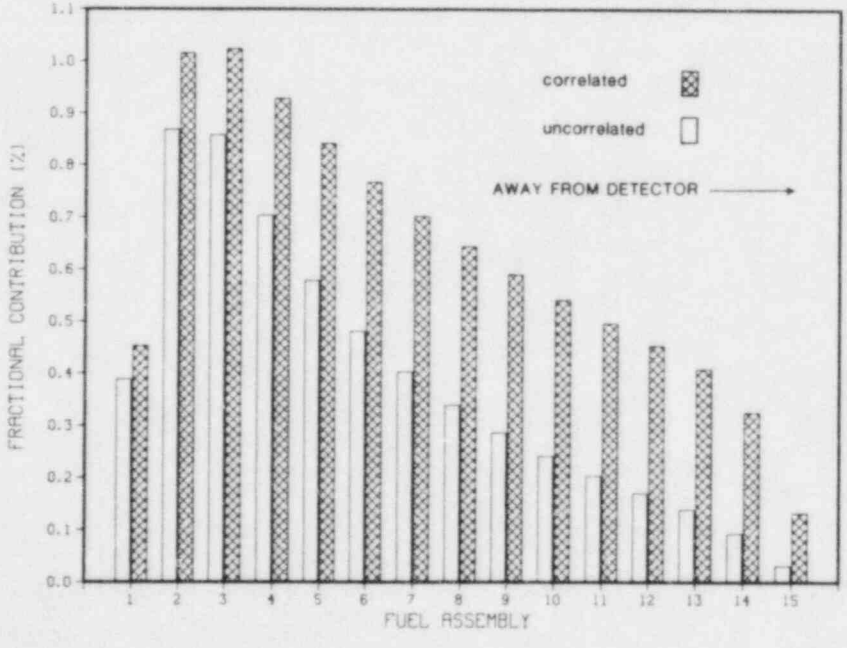

Fig. 24. Fractional contribution to the total ex-core detector response from fuel assembly vibrations along the symmetry axis for case 5 (end of cycle, burnable poison rods).

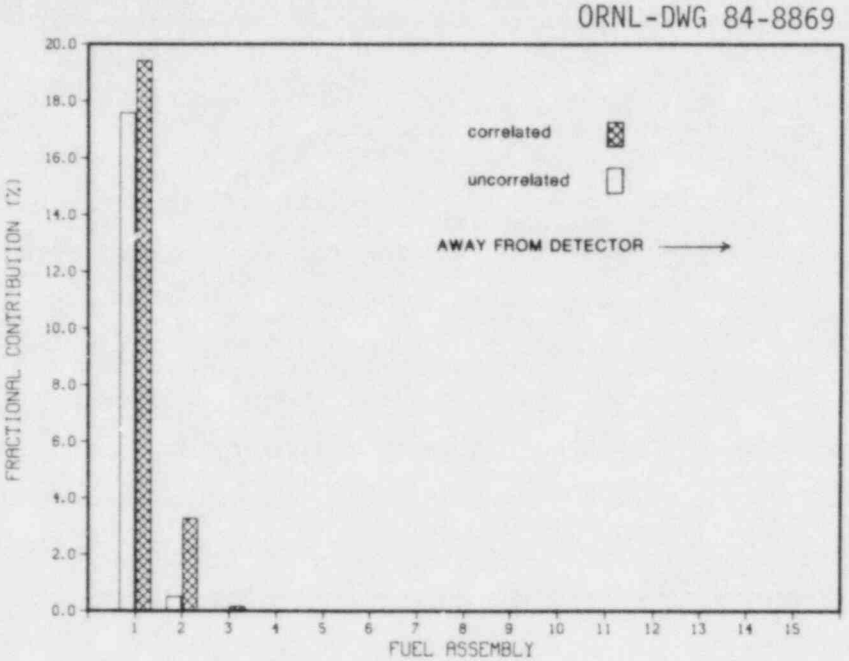

Fig. 25. Fractional contribution to the total ex-core detector response from fuel assembly vibrations along the symmetry axis for case 6 (beginning of cycle, burnable poison rods, $\nu\Sigma_f = 0$).

locations except at the edge of the core nearest the detector (fuel assembly 1). This indicates that both the total response (Table 1) and the spatial sensitivity of the ex-core neutron detectors are affected by the spatial correlation of the vibrations.

- As burnup increases (and soluble boron and burnable poison concentrations decrease correspondingly), the ex-core detectors become more sensitive to vibrations occurring in the central region of the core for both the BPR (cases 2 and 3) and NBPR (cases 4 and 5) cores.

- When equilibrium xenon concentration is assumed (cases 2 through 5), the ex-core detector becomes more sensitive to vibrations in

the central region of the core compared to the no xenon case (case 1).

- The nonfission case (case 6) overpredicts the contribution of fuel assembly vibrations on the core periphery and underpredicts the contribution of vibrations in the central region of the core compared to the fission cases (cases 1-5).

Vibrational characteristics of core internal structures are often inferred from phase relationships between ex-core detectors. The cross power spectral density (CPSD) magnitude and phase between cross-core (180° apart) detectors can be determined from a single detector adjoint calculation by assuming that the detectors and core are symmetric about the core center. The detector response for detector 1, δR_1 is identical to Eq. 14.

For the cross-core detector, the detector response δR_2 is

$$\delta R_2^{G_d}(r_{ds},\omega) = \sum_g \left\{ \phi^{+g}(r_{1s},\omega) \left[\sum_{g'} \left(\Sigma_w^{g',g} - \Sigma_c^{g',g} \right) \phi^{g'}(r_{1s}) \right] - \phi^{+g}(r_{2s},\omega) \left[\sum_{g'} \left(\Sigma_w^{g',g} - \Sigma_c^{g',g} \right) \phi^{g'}(r_{2s}) \right] \right\} dV \quad , \quad (17)$$

where r_{1s} and r_{2s} are mirror image spatial locations about the core centerline to r_1 and r_2, respectively (as shown in Fig. 26), and $\phi^+(r,\omega)$ is the detector adjoint for the detector position in the detector adjoint calculation. The CPSD between the two detectors is

$$\underset{\delta R_1 \delta R_2}{\mathrm{CPSD}(\omega)} = \delta R_1^{G_d *}(r_d,\omega)\ \delta R_2^{G_d}(r_{ds},\omega)$$

where * denotes the complex conjugate, and the phase is

$$\Theta_{\delta R_1 \delta R_2} = \tan^{-1}\left(\mathrm{CPSD}_{\delta R_1 \delta R_2}(\omega) \right) \quad .$$

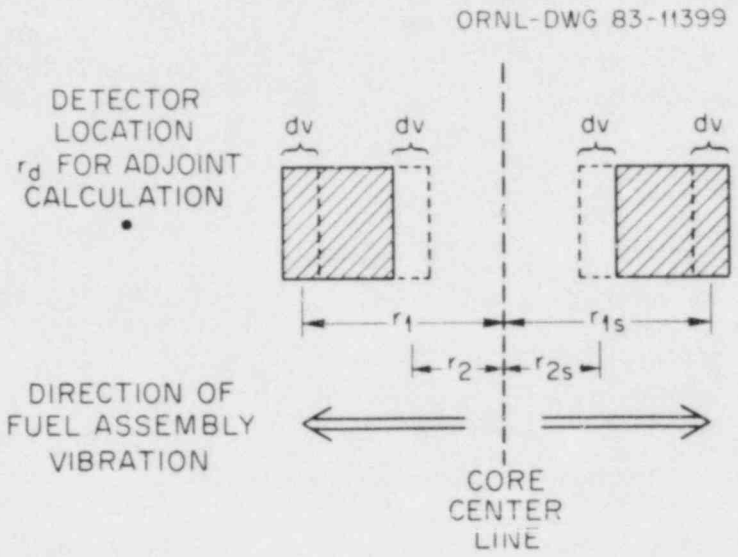

Fig. 26. Method of calculating the CPSD for two symmetrically located detectors for fuel assembly vibrations.

Typical CPSD magnitudes between cross-core detectors normalized to the mean reaction rate in the detectors (NCPSDs) and phase plots are shown in Figs. 27 and 28, respectively. As expected, the NCPSD is symmetrical about the core centerline and the detectors are more sensitive to vibrations on the core periphery compared to the center of the core. The phase shifts indicate that the detectors are from ±90° to ±180° out of phase, with a phase of exactly ±180° occurring only for the central fuel assembly (assembly 8). These large phase shifts can be attributed to a combination of the phase shifts due to the detector adjoints (Figs. 13-17), the 180° out-of-phase Langevin sources on each side of the fuel assembly, and the magnitude and gradient of the detector adjoint and static flux through which the assembly moves.

4.2.4 Results of Coolant Boiling Calculations

The ex-core detector response to coolant boiling (moderator density fluctuations) was determined by utilizing the techniques previously discussed, and the Langevin source described in Sect. 4.2.2. As in the fuel

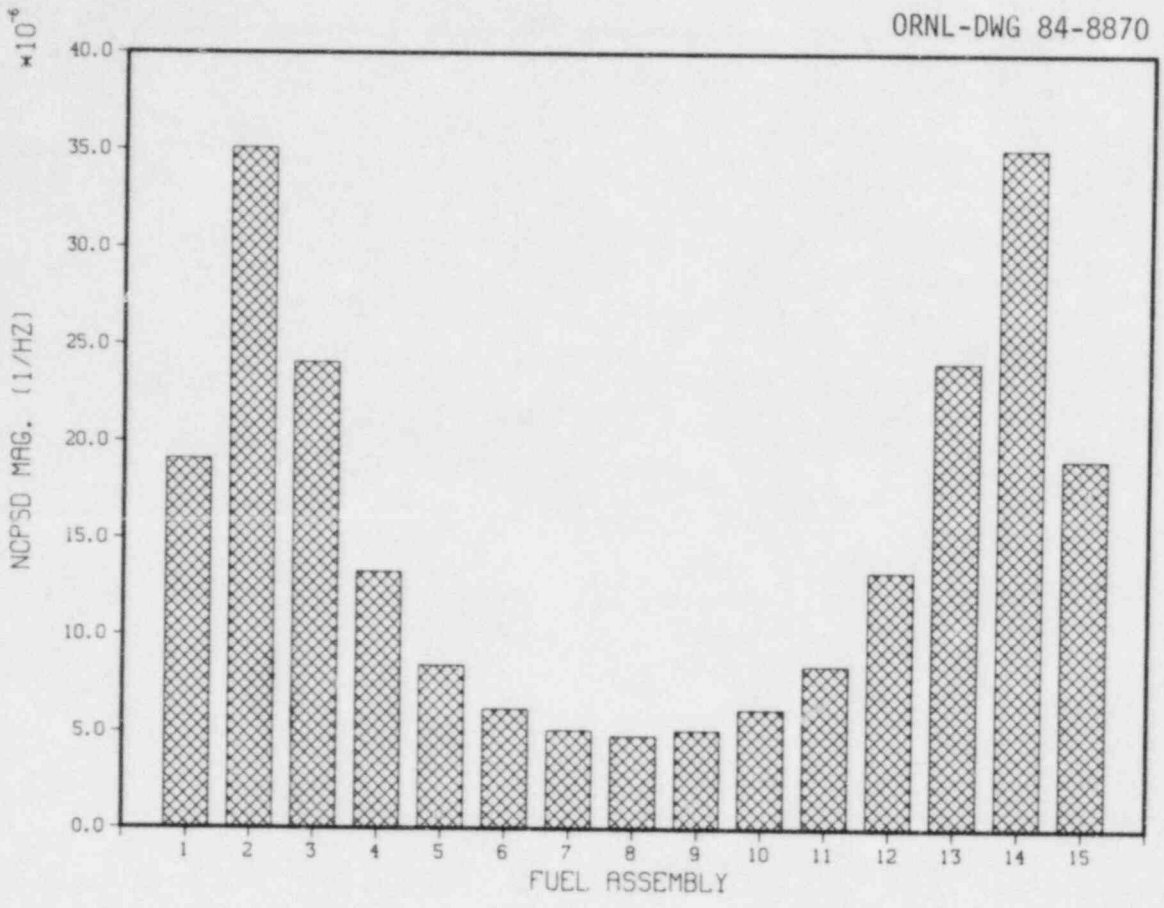

Fig. 27. CPSD Magnitude normalized to the mean reaction rate (NCPSD) between two symmetrically located detectors due to fuel assembly vibrations along the symmetry axis.

assembly vibrations, the total detector response to equal magnitude coolant density fluctuations in all fuel assemblies was calculated for cases 1 through 6 under the assumptions of spatially correlated or uncorrelated boiling. The results, normalized to the mean detector reaction rate per fractional density change ($\delta\rho/\rho_o$), are summarized in Table 2.

We made the following observations:

- Spatially correlated coolant boiling yields a total scale factor (detector response per fractional density change) about one order of magnitude larger than spatially uncorrelated boiling.

ORNL-DWG 84-8871

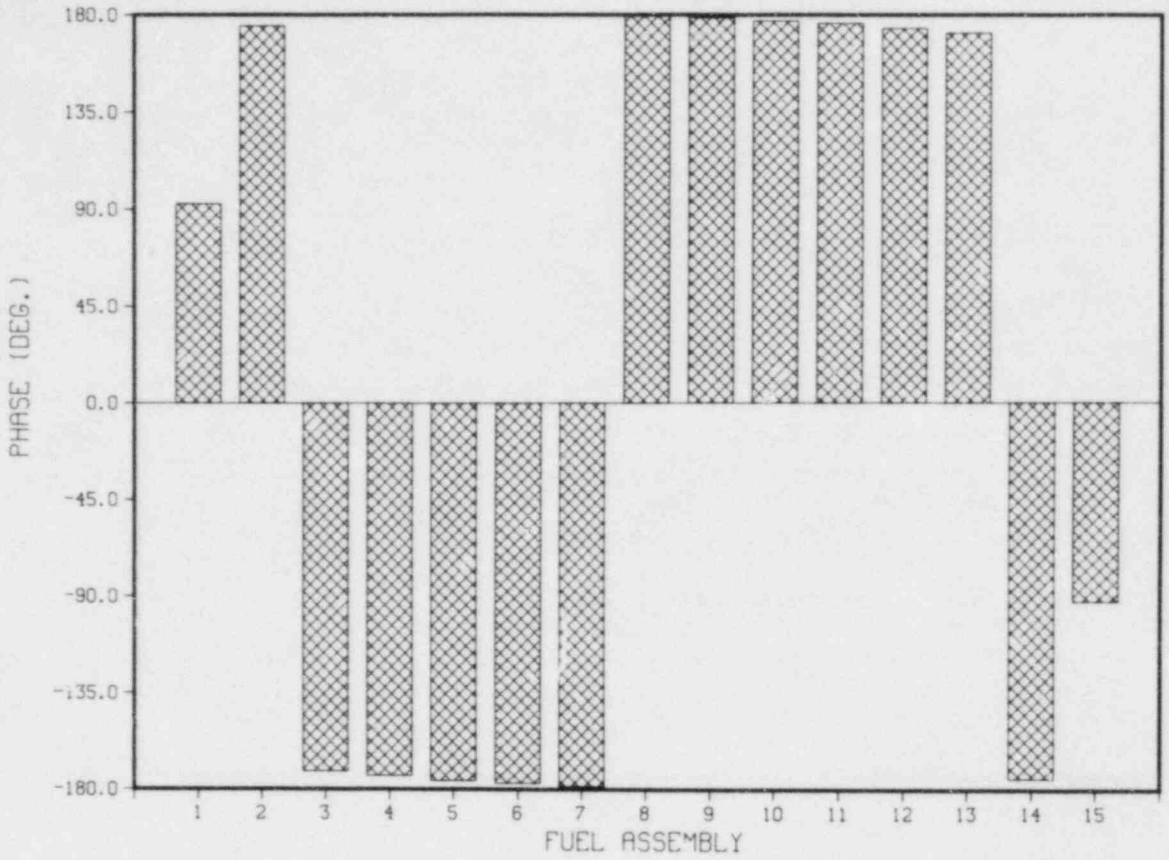

Fig. 28. Phase between two symmetrically located detectors due to fuel assembly vibrations along the symmetry axis.

- The detector response to boiling increases with increasing burnup (and decreasing boron concentration) even if the amount of boiling remains constant. These increases are about 15% greater for NBPR cores compared to BPR cores.

- Over a fuel cycle the calculated increases in the scale factors for boiling are 30 to 50% smaller than the expected increases in the fuel assembly vibration scale factors.

The ex-core detector response to boiling in individual fuel assemblies was calculated for cases 1 through 5, and the fractional contributions to the total signal for assemblies lying on the symmetry axis are

Table 2. Calculated ex-core detector scale factors for moderator boiling in a Westinghouse PWR

	Total scale factors[a]					
	Beginning of cycle		End of cycle		% increase	
	BPR[b]	NBPR[c]	BPR	NBPR	BPR	NBPR
correlated	1.1	0.90	1.3	1.2	18	33
uncorrelated	0.12	0.099	0.14	0.13	13	29

[a]Units are NRMS per % moderator density change normalized the mean detector response. All fuel assemblies assumed to have the same amount of boiling.

[b]BPR - burnable poison rods.

[c]NBPR - no burnable poison rods.

presented in Figs. 29-33 respectively. As in the fuel assembly vibrations, we found the following:

- Correlated boiling in individual assemblies contributes more to the total detector response than does uncorrelated boiling for all fuel assembly locations except at the edge of the core nearest the detector.

- As burnup increases and boron concentration decreases, the ex-core detectors become increasingly sensitive to boiling in the central region of the core for both the BPR and NBR cases.

- The equilibrium xenon cases (cases 2 and 4) show increased ex-core detector response to boiling in the central regions compared to the no-xenon case.

The CPSD and phase between cross-core detectors were determined by assuming that the detectors and core compositions are symmetric about the

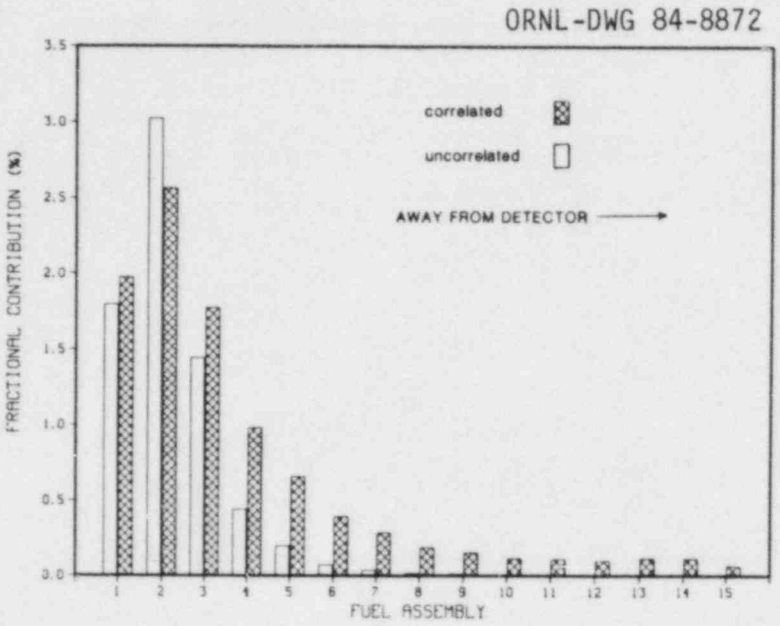

Fig. 29. Fractional contribution of moderator boiling in fuel assemblies along the symmetry axis to the total ex-core detector response for case 1 (beginning of cycle, no burnable poison rods, no xenon).

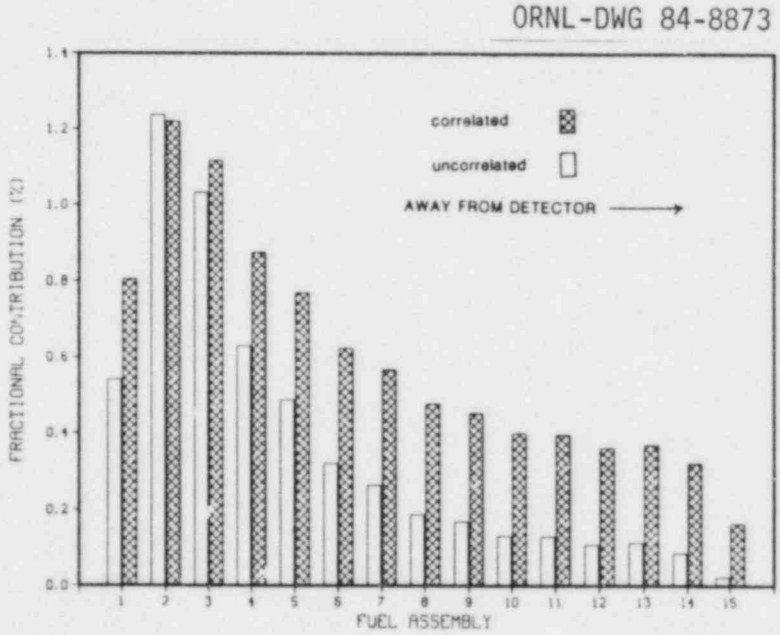

Fig. 30. Fractional contribution of coolant boiling in fuel assemblies along the symmetry axis to the total ex-core detector response for case 2 (beginning of cycle, no burnable poison rods, equilibrium xenon).

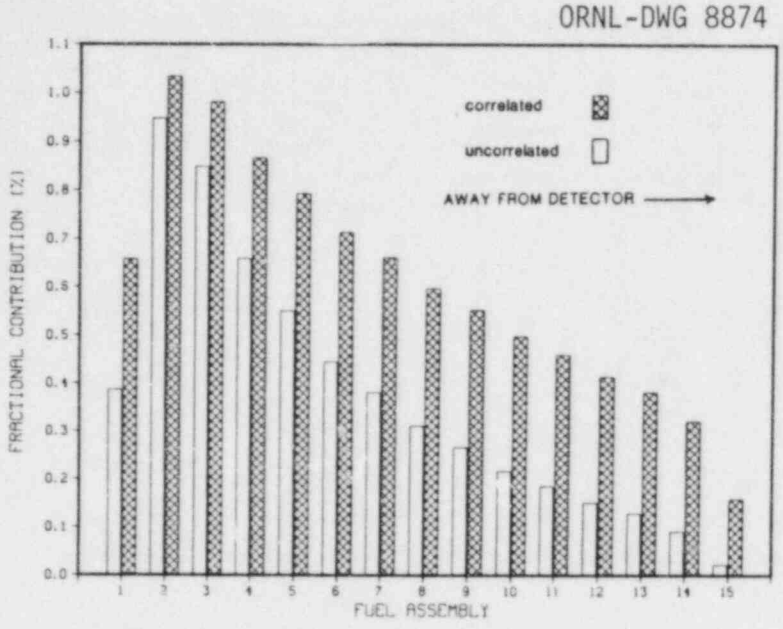

Fig. 31. Fractional contribution of coolant boiling in fuel assemblies along the symmetry axis to the total ex-core detector response for case 3 (end of cycle, no burnable poison rods equilibrium xenon).

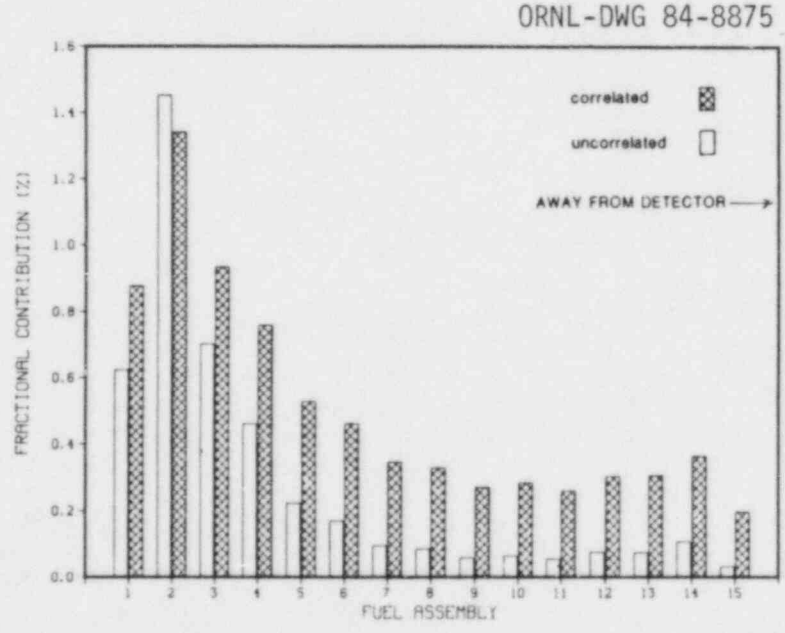

Fig. 32. Fractional contribution of coolant boiling in fuel assemblies along the symmetry axis to the total ex-core detector response for case 4 (beginning of cycle, burnable poison rods, equilibrium xenon).

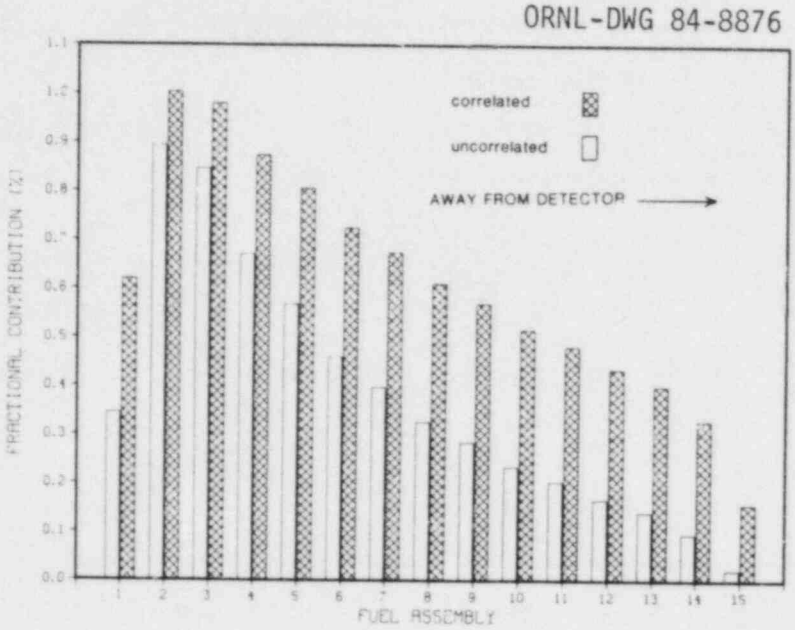

Fig. 33. Fractional contribution of coolant boiling in fuel assemblies along the symmetry axis to the total ex-core detector response for case 5 (end of cycle, burnable poison rods, equilibrium xenon).

core center. The detector response for the first detector was calculated using Eq. 16, and the second detector response was determined from the original adjoint calculation by

$$\delta R_2^{G_d}(r_d,\omega) = \sum_g \phi^{+g}(r_s,\omega) \sum_{g'} \left(\Sigma_{w_1}^{g',g} - \Sigma_{w_2}^{g',g} \right) \phi^{g'}(r_s) dV \qquad (18)$$

where r_s is the spatial location symmetric about the core center line to r as shown in Fig. 34.

Plots of typical NCPSD magnitude and phase for cross-core detectors are shown in Figs. 35 and 36 respectively. The NCPSD magnitude shows the expected symmetrical distribution similar to that exhibited by fuel assembly vibrations. The phase, however, is exactly zero only for the central fuel assembly, with maximum phase shifts of up to 20° occurring for assemblies located on the core periphery. The difference in phase shifts for boiling compared to fuel assembly vibration is the result of the single Langevin source (as opposed to the two Langevin sources with

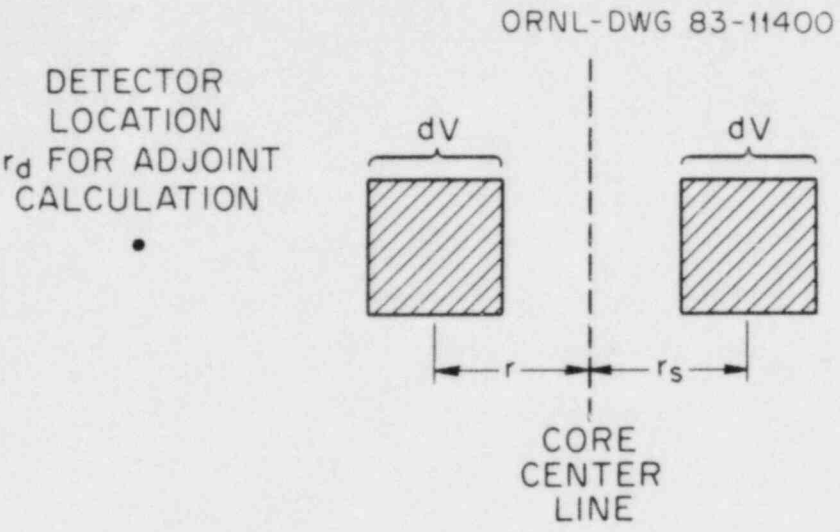

Fig. 34. Method of calculating the CPSD between two symmetrically located detectors for coolant boiling.

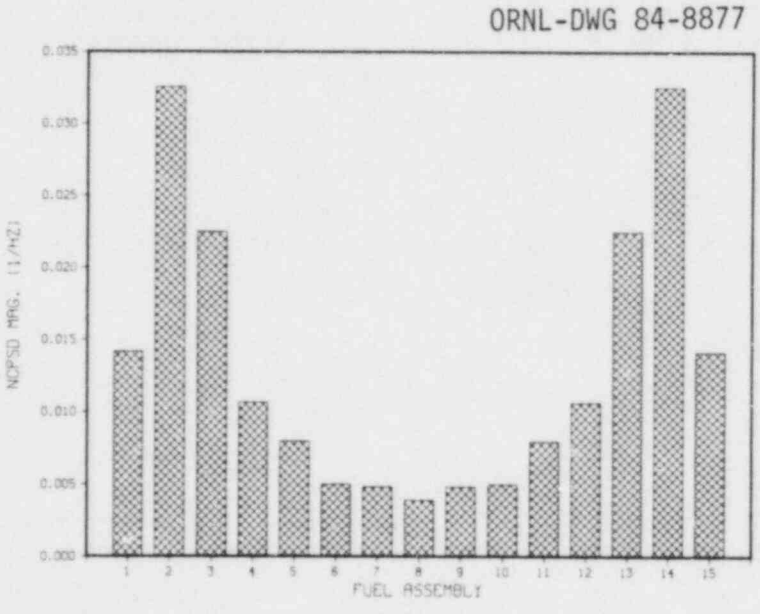

Fig. 35. Normalized cross power spectral density (NCPSD) magnitude between two symmetrically located detectors with boiling along the symmetry axis.

180° phase shifts for fuel assembly vibration). The resulting phase shifts depend only on the phase of the detector adjoint since the ex-core detector responses are not determined by a perturbation moving through gradients of the detector adjoint or static flux.

ORNL-DWG 84-8878

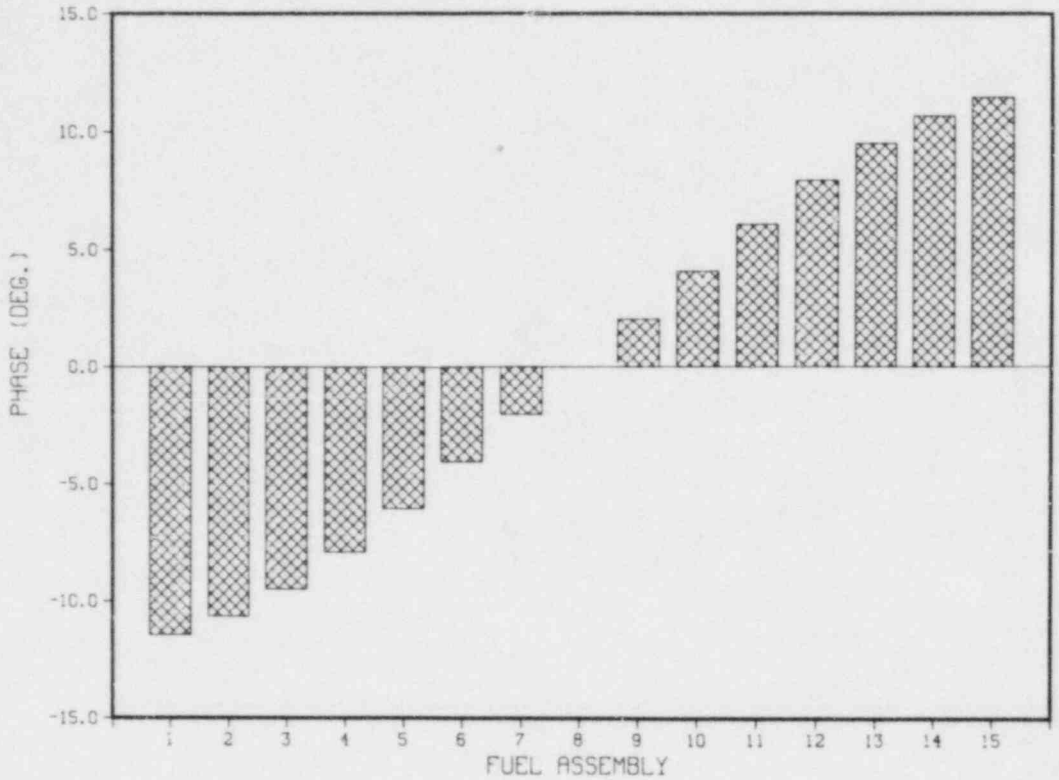

Fig. 36. Phase between two symmetrically located detectors due to boiling along the symmetry axis.

4.3 COMPARISON OF CALCULATED RESULTS WITH SEQUOYAH-1 NEUTRON NOISE MEASUREMENTS

Measurements of ex-core neutron detector noise were performed at Sequoyah-1, an 1150-MW(e) Westinghouse PWR, during the first fuel cycle. The noise data were obtained from an on-line surveillance system and from periodic FM tape recordings which were analyzed off-line. Details of these measurements are included in refs. 34-36 and will not be discussed here.

A typical power spectral density normalized to the mean detector reaction rate (NPSD) of the ex-core neutron noise shows a resonance at ~3.5 Hz as presented in Fig. 37. This resonance has been observed in

ORNL-DWG 84-8879

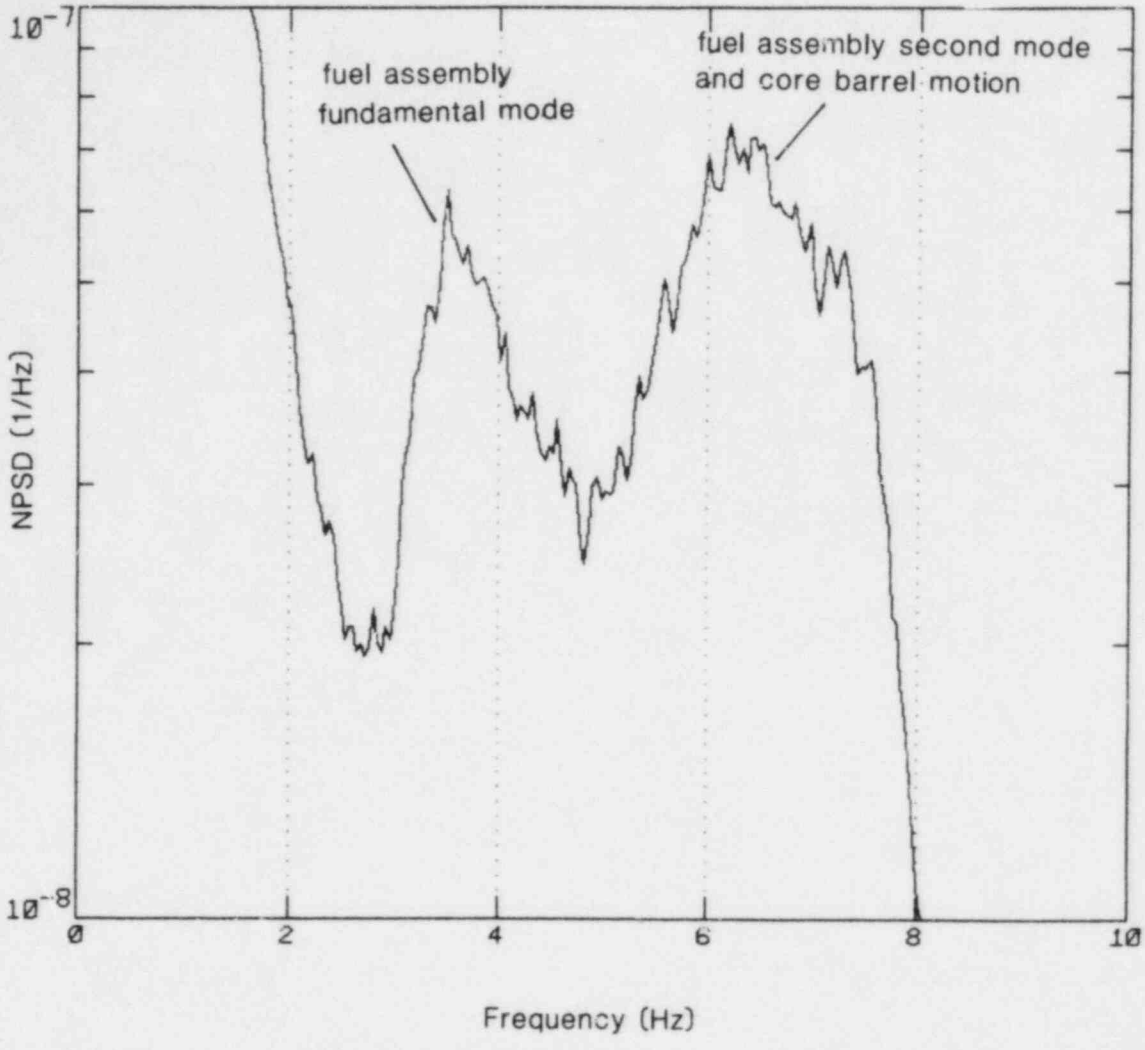

Fig. 37. Experimentally measured ex-core neutron detector normalized power spectral density (NPSD) from the Sequoyah-1 PWR.

many PWRs at approximately the same frequency, and the accepted interpretation is that it results from first-mode (natural frequency) vibrations of the fuel assemblies.[11,29,30]

The normalized root mean square (NRMS) was obtained from the NPSDs over the 2.5- to 4.0-Hz range and plotted versus boron concentration in Fig. 38. The NRMS versus boron concentration plot is nearly linear, and the NRMS increases with decreasing boron concentration. A linear

ORNL-DWG 84-8880

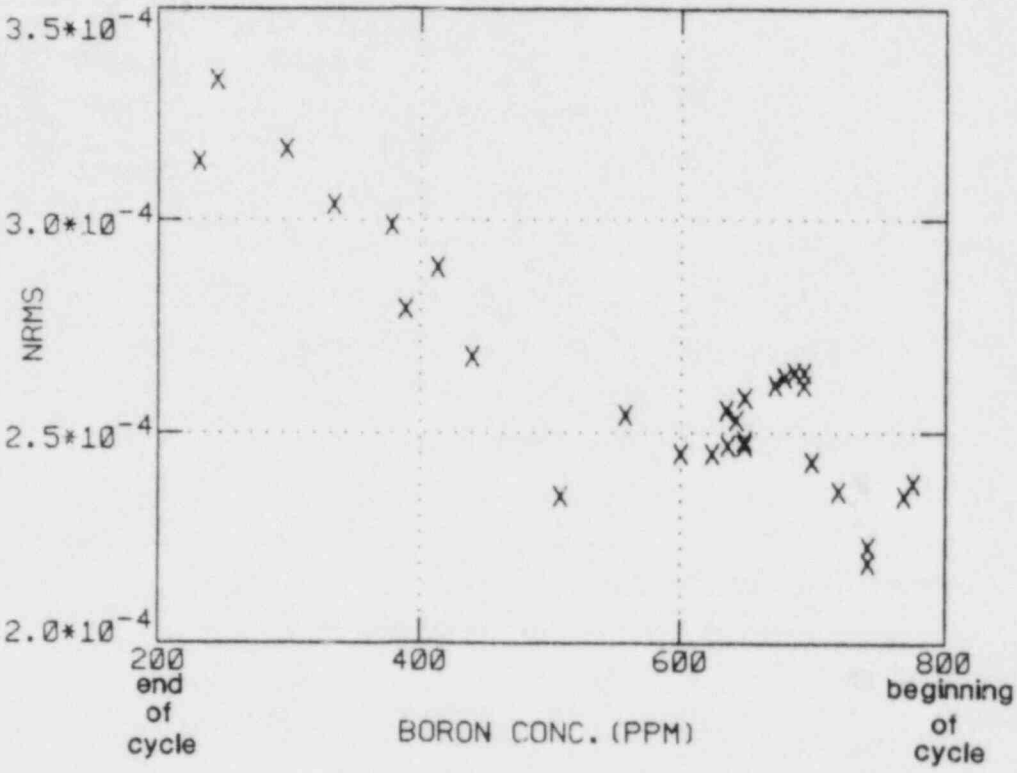

Fig. 38. Experimentally measured ex-core neutron detector normalized root mean square (NRMS) versus boron concentration during the first fuel cycle of the Sequoyah-1 PWR.

behavior of neutron noise at low frequencies (<1 Hz) versus boron concentration has been predicted for fuel assembly vibrations using point kinetics by Saxe[18] and Meyer.[37] Temperature (moderator density) fluctuations have been shown to produce a nonlinear noise dependance of neutron noise on the boron concentration by other workers.[38] The increase in the neutron noise observed at Sequoyah-1 was ~60% for the range of soluble boron concentrations presented, which agrees well with the predicted 58% increase in the scale factor for fuel assembly vibrations over this same range of boron concentrations presented in Table 1. The increase in the neutron noise is much larger than could be accounted for by the ~18% increase in the scale factor for coolant boiling (moderator density fluctuations). We therefore concluded that the increase in the neutron noise in the 2.5- to 4.0-Hz region is completely accounted for by the

increased detector response to fuel assembly vibration, and that the amplitude of the vibrations did not increase over the fuel cycle.

Increases in the neutron noise in this frequency range have also been observed in other PWRs.[10,30,39] These increases in noise have usually been accompanied by a 1- to 2-Hz shift in the fuel assembly resonant frequency,[10,30] which has been interpreted as an increase in assembly vibrational amplitude due to relaxation of grid spacer springs. At Sequoyah-1 the fuel assembly resonant frequency has been observed to shift <0.5 Hz over the range of boron concentrations presented in Fig. 38, and we concluded that the increased neutron noise at Sequoyah-1 was not the result of grid spacer spring relaxation.

The amplitude of fuel assembly vibrations (assuming that all fuel assemblies vibrate with the same amplitude) can be inferred from experimental data using the calculated scale factors (S.F.) in Table 1:

$$\delta X(\text{cm RMS}) = \frac{\delta R(\text{NRMS})}{\text{S.F}(\text{NRMS/cm})}$$

where δR is the measured neutron noise NRMS and δX is the inferred fuel assembly amplitude RMS. These scale factors were applied to the neutron noise NRMS at Sequoyah-1 (Fig. 38) for BOC and EOC conditions, and the results are summarized in Table 3. The inferred fuel assembly vibrational amplitudes of 0.36×10^{-4} to 3.1×10^{-4} cm RMS (~0.014 to

Table 3. Fuel assembly vibrational amplitudes inferred from measured ex-core detector neutron noise at Sequoyah-1

	Inferred amplitudes (10^{-4} cm RMS)*	
	Beginning of cycle	End of cycle
Correlated	0.37	0.36
Uncorrelated	3.1	3.1

*All fuel assemblies are assumed to vibrate with the same amplitude. Scale factors for BPR cases (Table 1) were utilized.

0.12 mils RMS) compares reasonably well with the amplitudes of 2.5×10^{-4} and 4×10^{-4} cm (0.1 mils and 0.16 mils RMS) reported in refs. 10 and 40 respectively.

4.4 SUMMARY OF RESULTS

The following paragraphs summarize the significant results of the previous sections:

1. Ex-core neutron detectors are more sensitive to fluctuating neutron sources at all core locations than previous calculations indicated. The spatial sensitivity for these sources (detector adjoint) does not change significantly with burnup and boron concentration.

2. Delayed neutrons cause large (~20°) phase shifts in the detector adjoint at 3 Hz, indicating that static shielding techniques are not appropriate for kinetic analysis of the ex-core detector spatial sensitivity to in-core perturbations.

3. Fuel assembly vibrations and boiling in locations other than the core periphery can contribute significantly to ex-core detector response. Previous calculations underpredict the scale factor for fuel assembly vibrations (and therefore overpredict the inferred amplitude of vibration) and the contribution of vibrations in locations other than the core periphery.

4. The neutron noise induced by fuel assembly vibrations or coolant boiling increases with increasing burnup (and decreasing boron concentration) without increases in the vibrational amplitudes or the amount of boiling.

5. The predicted changes in neutron noise resulting from burnup were observed at Sequoyah-1 during the first fuel cycle. The inferred amplitudes of fuel assembly vibrations did not change over the fuel cycle and compare well with values reported in the open literature.

5. FEASIBILITY OF DETECTING ANOMALOUS FUEL ASSEMBLY VIBRATIONS AND BOILING USING EX-CORE NEUTRON DETECTORS

The ability of a noise analyst to differentiate between normal and abnormal changes in neutron noise is a fundamental requirement in the diagnosis of anomalies. In the previous section, the calculated ex-core detector responses were used to interpret observed changes in neutron noise as normal (not indicative of an anomalous condition). In many cases, the analyst needs to know whether noise techniques are sufficiently sensitive to detect a postulated anomaly. For example, can ex-core neutron noise be used to detect abnormal fuel assembly vibrations on the core periphery (such as might be induced by baffle jet flow)?

The feasibility of detecting anomaly depends on the following information:

a. The location of the anomaly and the magnitude of the scale factor relating the perturbation at that location to the detector reponse.

b. The statistical uncertainty in the analysis technique.

c. Normal changes in the noise signal due to plant operation.

d. The "background" noise level due to instrumentation noise or to perturbations which are not anomalous.

As an example of a possible application of the calculated detector responses, we will determine the ex-core detector sensitivity to abnormal fuel assembly vibrations on the core periphery such as might occur due to baffle jetting.

5.1 FEASIBILITY OF DETECTING BAFFLE JET FLOW-INDUCED VIBRATIONS

The following assumptions were made in this analysis:

1. The location of the baffle jet-induced fuel assembly vibration is known (since the location of the baffle joints are known).

2. Baffle jet flow excites the fundamental mode of fuel assembly vibration at 3 Hz.*

3. The normal fuel assembly vibrations are spatially uncorrelated with amplitudes of 0.12 mils RMS.

4. The neutron noise dependence on boron concentration and burnup is known (from Table 1).

5. The normal range of fluctuations is $\pm 5 \times 10^{-5}$ NRMS at a given boron concentration as shown in Fig. 39.

6. The analysis statistical error is small and therefore can be neglected (this can be controlled through analysis of long-term records).

For baffle jet flow at fuel assembly location P-13 (see Fig. 5), the scale factor for case 2 (BOC, BPR) is 3.27×10^{-2} NRMS/cm, and for case 3 (EOC, BPR) is 2.5×10^{-2} NRMS/cm. The increase in noise that this fuel assembly must induce to be classified abnormal is a minimum of 1.0×10^{-4} NRMS ($2 \times 5 \times 10^{-5}$ from Fig. 39). The predicted increases in vibrational amplitudes needed in order to produce detectable anomalous noise levels are summarized in Table 4 and indicate that the fuel assembly must

*Recent measurements[41] have indicated that baffle jet flow may excite fuel assembly vibrations at frequencies other than 3 Hz. It is not known if these frequencies are vibrations of the fuel assembly as a whole or vibration of individual fuel pins.

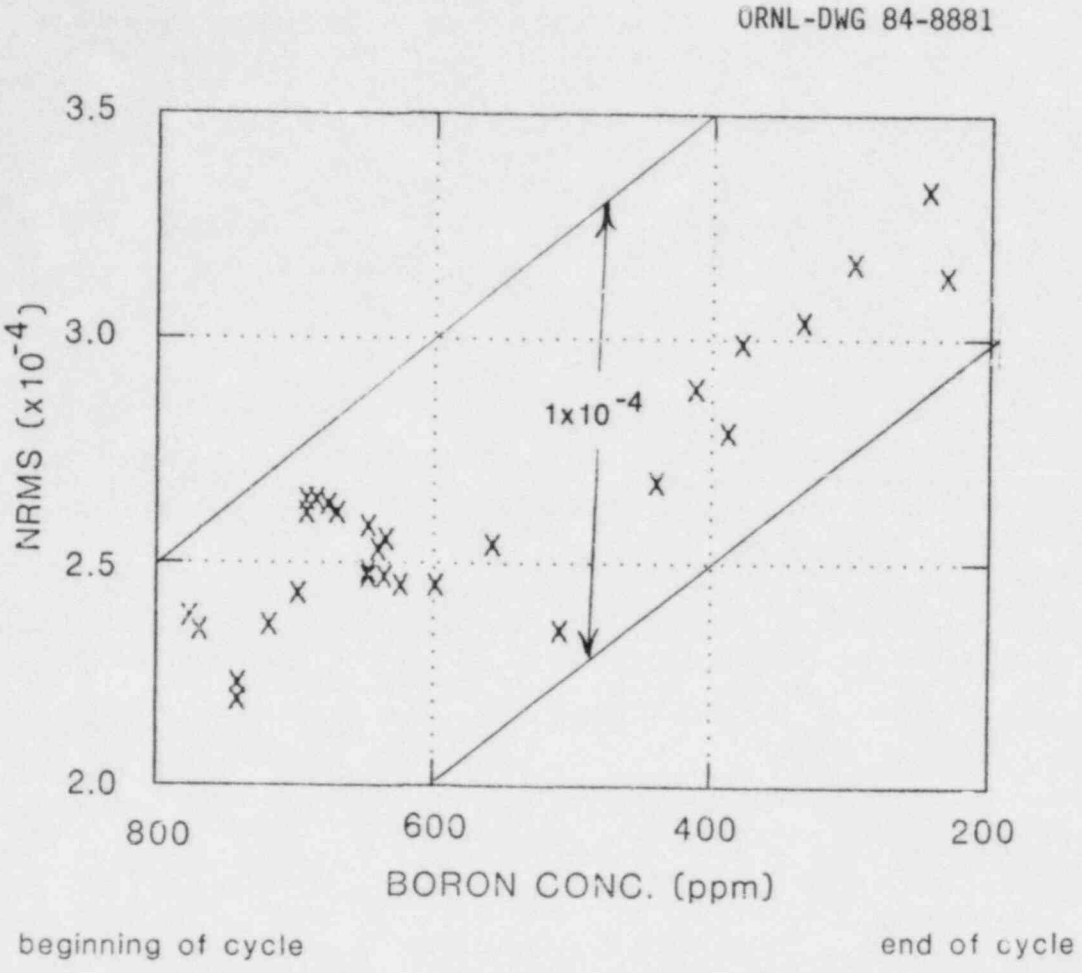

Fig. 39. Normal range of ex-core detector neutron noise over a fuel cycle for the Sequoyah-1 PWR.

vibrate ~10 times its normal amplitude in order to be detected. The total amplitude of vibration is the sum of the vibration increase (due to baffle jet flow) and the normal amplitude of 3.1×10^{-4} cm (0.12 mils). These results indicate that since the fuel assembly spacings are 0.10 cm (~39 mils), baffle jet flow-induced fuel assembly vibrations might be detected with ex-core neutron detectors before surrounding assemblies are damaged. However, normal day-to-day fluctuations and the dependence on boron concentration of the neutron noise must be known. Note that the application of crest factors[8] could increase the values shown in Table 4 by as much as a factor of three (for the 99% confidence level).

Table 4. Minimum amplitude of baffle jet flow-induced fuel assembly vibration needed to be detected with ex-core neutron detectors

	Amplitude increase* (cm × 10^{-3} RMS)	Total amplitude (cm × 10^{-3} RMS)
BOC, BPR	3.0	3.3
EOC, BPR	3.8	4.1

*Fuel assembly location P-13 (from Fig. 5) to produce an increase in the ex-core neutron noise of 1.0×10^{-4} NRMS.

5.2 COMPARATIVE SENSITIVITY OF TWO NOISE MONITORING SYSTEMS

The previous section described the detection of an anomaly based on a knowledge of the normal fluctuations in the neutron noise and the dependence of the neutron noise on boron concentration and burnup. By utilizing the information a "smart" automated monitoring system could be developed to differentiate between an anomalous condition and normal changes in the neutron noise. On the other hand, a simple RMS meter type device could be developed with a single alarm level to detect the anomalous condition. Such a device would require an alarm level high enough so that normal changes due to plant operation and boron concentration changes would not produce false alarms.

The problem, then, is to determine how much sensitivity for detecting the anomalous condition is sacrificed by using the simple device. Using the data of Fig. 39, it is evident that the RMS meter alarm threshold for anomalous fuel assembly vibrations must be set at $\sim 3.5 \times 10^{-4}$ NRMS. The baffle jet problem discussed in the previous section was reanalyzed assuming that at BOC the fuel assembly must induce a detector response of 3.5×10^{-4} NRMS and, therefore, a noise increase of $\sim 2.0 \times 10^{-4}$ NRMS over normal levels. The minimum amplitudes needed to produce an alarm under these assumptions are summarized in Table 5.

Table 5. Minimum amplitude of baffle jet flow-induced fuel assembly vibration in order to be detected using a simple monitoring device

	Amplitude increase[a] ($\times 10^{-3}$ cm RMS)	Total amplitude ($\times 10^{-3}$ cm RMS)
BOC, BPR	6.1[b]	6.4
EOC, BPR	3.8[c]	4.1

[a]Fuel assembly location P-13 (see Fig. 5).

[b]Required to produce an increase of 2.0×10^{-4} NRMS ex-core neutron noise.

[c]Required to produce an increase of 1.0×10^{-4} NRMS ex-core neutron noise.

The results of this analysis show that the simple device is ~50% less sensitive than the smart system (i.e., under BOC conditions the fuel assembly vibrational amplitude must be larger by a factor of two to produce an alarm with the simple device). This is because in the simple device there is no compensation for the normal increases in the ex-core neutron noise caused by burnup and boron concentration changes.

6. SUMMARY AND RECOMMENDATIONS

We accomplished the following tasks in this work:

- Developed a methodology for calculating the ex-core neutron detector response to in-core perturbations.
- Utilized this methodology to predict the detector response to fuel assembly vibrations and in-core boiling.
- Interpreted changes in experimentally measured neutron noise data.
- Applied the calculated detector responses to determine the feasibility of detecting an in-core anomaly.
- Utilized the calculated detector responses to show how the sensitivity for detecting an anomaly with automated noise surveillance and diagnostic systems can be improved.

In the course of this investigation several areas needing additional research became obvious, and we make the following recommendations

1. Succeeding fuel cycles of Sequoyah-1 should be analyzed to interpret neutron noise measurements and characterize normal long term neutron noise behavior.

2. Calculations should be performed at higher frequencies in order to interpret neutron noise changes associated with higher fuel assembly vibrational modes.

REFERENCES

1. D. N. Fry, R. C. Kryter, and J. C. Robinson, "Analysis of Neutron Density Oscillations Resulting from Core Barrel Motion in the Palisades Nuclear Power Plant," ORNL-TM-4570 (1974).

2. J. A. Thie, "Theoretical Considerations and Their Application to Experimental Data in the Determination of Reactor Internals' Motion from Stochastic Signals," *Ann. Nucl. Energy* 2, 253 (1975).

3. "Reactor Internal Noise Monitoring Tests," Consumers Power Co. Report to the U.S. Nuclear Regulatory Commission, Docket 50-255 (April 27, 1978).

4. "Reactor Internal Noise Monitoring Tests," Consumers Power Co. Report to the U.S. Nuclear Regulatory Commission, Docket 50-255 (January 26, 1976).

5. M. Calcagno and F. Cioli, "Trino Vercellese Nuclear Power Plant In-Service Monitoring of Core Structures and Reactor Internals by Neutron Noise Measurements," *Ente Nazionale per l'Energia Ellettrica* Rome (August 1976).

6. A. Brillon and C. Puyal, "Mechanical Surveillance of French PWRs," Sixth Conference on Structural Mechanics in Reactor Technology (SMIRT-6), Paris (August 1981).

7. B. J. Verna, "Nuclear Power Experience - Vol. PWR-2," Nuclear Power Experience, Inc. (1977).

8. J. C. Robinson, F. Shahrokhi, and R. C. Kryter, "Calculation of the Scale Factor for Inference of Pressurized Water Reactor Core Barrel Motion from Neutron Noise Spectral Density," *Nucl. Technol.* 40, 35 (1978).

9. P. Bernard et al., "Quantitative Monitoring and Diagnosis of French PWRs Internal Structures Vibrations by Ex-Core Neutron Noise and Accelerometers Analysis," *Prog. Nucl. Energy* 9, 465 (1982).

10. C. W. Mayo and R. T. Currie, "Neutron Noise Monitoring of Pressurized Water Reactor Internal Vibrations," *Prog. Nucl. Energy.* 1, 363 (1977).

11. W. J. Bryan, "Digital Analysis Techniques Used in Nuclear Fuel Vibration Analysis," ASME Conference on Flow Induced Vibration, San Francisco, p. 91 (June 1979).

12. "Comprehensive Vibration Assessment Program for Reactor Internals During Preoperational and Initial Startup Testing," Regulatory Guide 1.20, U.S. Nuclear Regulatory Commission (May 1976).

13. "Loose-Part Detection Program for the Primary System of Light-Water-Cooled Reactors," Regulatory Guide 1.133, U.S. Nuclear Regulatory Commission (May 1981).

14. W. J. Bailey, K. H. Rising, and M. Tokar, "Fuel Performance Annual Report for 1980," NUREG/CR-2410 (PNL-3953) (1981).

15. M. W. Crump and J. C. Lee, "Calculation of Spatial Weighting Factors for Ex-Core Neutron Detectors," *Nucl. Technol.* 41, 87-96 (1978).

16. Y. Fujita and H. Ozaki, "Neutron Noise Monitoring of Reactor Core Internal Vibrations at PWRs in Japan," *Prog. Nucl. Energy* 9, 423-436 (1982).

17. H. Tochihara, E. Ochiai, and T. Hasegawa, "Reevaluation of Spatial Weighting Factors for Ex-Core Neutron Detectors," *Nucl. Technol.* 58, 310-317 (1982).

18. R. F. Saxe, K. Verghese, and P. G. Ibrahim, "Variation of Neutron-Density Noise During Core Life in a Pressurized Water Reactor," *Nucl. Sci. Eng.* 75, 190-191 (1980).

19. I. Pazit, "Two-Group Theory of Noise in Reflected Reactors with Application to Vibrating Absorbers," *Ann. Nucl. Energy* 5, 185-196 (1978).

20. I. Pazit, and G. Th. Analytis, "Theoretical Investigation of the Neutron Noise Diagnostics of Two-Dimensional Control Rod Vibrations in a PWR," *Ann. Nucl. Energy* 7, 171-183 (1980).

21. S. J. Lee and R. W. Albrecht, "The Use of Neutronic Fluctuations to Locate a Vibrating Control Rod in a Pressurized Water Reactor Model," *Nucl. Sci. Eng.* 83, 427 (1983).

22. G. Th. Analytis, "Analysis of the Neutron Response to Axially Propagating Perturbations in a Heterogeneous Lattice of Cylindrical Fuel Elements Via the Two-Group Slowing-Down Model," *Ann. Nucl. Energy* 9, 417 (1982).

23. G. Th. Analytis, "A Semi-Analytical Solution of the Two-Group Feinberg-Golanin Kinetic Adjoint Equations for a Heterogeneous Lattice of Cylindrical Fuel Elements," *Ann. Nucl. Energy* 9, 591 (1982).

24. F. J. Sweeney and J. C. Robinson, "Relative Importance of Attenuation and Reactivity Effects in Explaining Local and Global BWR Neutron Noise," *Trans. Am. Nucl. Soc.* 34, 802 (1980).

25. M. M. R. Williams, *Random Processes In Nuclear Reactors*, Oxford: Pergammon Press Ltd. (1974).

26. G. I. Bell and S. Glasstone, *Nuclear Reactor Theory*, New York: Van Nostrand Reinhold Co. (1970).

27. J. S. Bendat and A. G. Piersol, *Random Data: Analysis and Measurement Procedures*, New York: Wiley-Interscience (1971).

28. A. R. Buhl et al., "A User's Manual for TASK, a Generalized One-Dimensional Transport and Diffusion Kinetics Code," ORNL-TM-3811 (1972).

29. L. A. Walton, F. E. Stokes, and J. N. Black, "Fuel Assembly Dynamic Behavior," *Trans. Am. Nucl. Soc.* 24, 354 (1976).

30. D. Wach and R. Sunder, "Improved PWR Neutron Noise Interpretation Based on Detailed Vibration Analysis," *Progr. Nucl. Energy* 1, 309 (1977).

31. W. W. Engle, Jr., "A User's Manual for ANISN a One-Dimensional Discrete Ordinates Transport Code with Anisotropic Scattering," UCC-ND K-25 Report K-1693, (1967).

32. J. P. Renier, *Multi-Group, Multi-Dimensional Investigations of the Power Spectral Densities of the Georgia Tech Research Reactor and the fast Thermal Argonaut Reactor*, Ph.D. dissertation, Georgia Institute of Technology (1976).

33. D. R. Vondy, P. B. Fowler, and G. W. Cunningham, III, "The BOLDVENTURE Computation System for Nuclear Reactor Core Analysis, Version III," ORNL-5711 (1981).

34. N. E. Clapp et al., "Advances in Automated Noise Data Acquisition and Noise Source Modeling for Power Reactors," *Prog. Nucl. Energy* 9, 493-504 (1982).

35. C. M. Smith, "A Description of the Hardware and Software of the PSDREC Continuous On-Line Reactor Surveillance System," NUREG/CR-3439, ORNL/TM-8862 (1983).

36. D. N. Fry et al., "Neutron Noise in Light-Water Reactors," NUREG/CR-3303, ORNL/TM-8774 (January 1984).

37. K. Meyer, "Zur Abhangigkeit der Spektraldichte des Leistungsrauschens von Druckwassereaktoren von der Borsaurekonzentration," *Kernenergie* 24, 347-348 (1980).

38. K. Meyer, "Zur Abbildung stochastischer Schwingungen von Arbeitskasseten eines DWR I", *Kernenergie* 25, 204-207 (1982).

39. J. P. Steelman and B. T. Lubin, "Analysis of Changes with Operating Time in the Calvert Cliffs Unit 1 Neutron Noise Signals," *Prog. Nucl. Energy* 1, 379-391 (1977).

40. F. E. Stokes and R. A. King, "PWR Fuel Assembly Dynamic Characteristics," Int. Conf. on Vibration in Nuclear Plants, Keswick, UK, May 9-12, 1978.

41. P. Bernard et al., "PWR Core Monitoring by Incore Noise Analysis," *Progr. Nucl. Energy* 9, 541 (1982).

APPENDIX A

ONE-DIMENSIONAL SLAB, FREQUENCY-DEPENDENT DISCRETE ORDINATES DETECTOR ADJOINT EQUATIONS WITH DELAYED NEUTRONS IN THE TASK COMPUTER CODE

APPENDIX A

ONE-DIMENSIONAL SLAB, FREQUENCY-DEPENDENT DETECTOR ADJOINT EQUATIONS WITH DELAYED NEUTRONS IN A MODIFIED VERSION OF THE TASK COMPUTER CODE

The TASK computer code[1] distributed by the Radiation Shielding Information Center (RSIC) at the Oak Ridge National Laboratory currently is written only to perform forward source or eigenvalue solutions of the multi-group, frequency-dependent, discrete ordinates (S_n) form of the Boltzmann transport equation. The TASK code was modified to solve the detector adjoint problems presented in Sect. 4.

The adjoint equations solved in the modified version of TASK are derived by applying the method of discrete ordinates[2] to Eq. 4 of Sect. 3. Scattering anisotropy up to order L is assumed by expanding the scattering components into L + 1 Legendre polynomials. The resulting equations solved in TASK for one-dimensional slab geometry are therefore:

$$\frac{\partial \phi^{\dagger}_{gd}}{\partial X \partial X}(X,\omega) + \frac{1}{\mu_d}\left(\sum_{g'=1}^{G} \sum_{d'=1}^{D} \left\{ \left[\Sigma_g + \frac{j\omega}{V_g} \right] \delta^{g}_{g'} \delta^{d}_{d'} \right.\right.$$

$$- \left[(1 - \beta_T)\, \chi_{g'} + \sum_{i=1}^{M} \frac{\lambda_i \gamma^{i}_{g'} \beta_i}{\lambda_i + j\omega} \right] (\nu\Sigma_f)_g W_{d'}$$

$$\left.\left. - \left[\sum_{\ell=0}^{L} \Sigma_s^{\ell}(g', g)\, P_\ell(\mu_d)\, P_\ell(\mu_{d'}) \right] W_{d'} \right\} \phi^{\dagger}_{g'd'} \right)(X,\omega)$$

$$= \frac{S^{\dagger}_{gd}(X_z,\omega)}{\mu_d} \quad \text{for} \quad \begin{matrix} g = 1,\ldots, G \\ d = 1,\ldots, D \end{matrix}$$

with

$\phi^{\dagger}_{gd}(X,\omega)$ = 0 for outgoing angles on the system boundary (vacuum boundary conditions)

where

δ^{m}_{ℓ} = 1, if $\ell = m$
0, if $\ell \neq m$

$S^{\dagger}_{gd}$ = the detector response function (Σ detector) for group g, angular segment d, and at position X_z;

$\phi^{\dagger}_{gd}$ = detector adjoint in group g and angular segment d;

μ_d = average x-direction cosine of the velocity vector of the neutrons;

W_d = weight of the angular segment d;

Σ_g = total cross section for group g;

γ^{i}_{g} = fraction of delayed neutrons of type i decaying into group g;

χ_g = fraction of prompt neutrons born in group g;

$(\nu\Sigma_f)_g$ = number of neutrons per fission times the fission cross section for group g;

$\Sigma^{\ell}_{s}(g',g)$ = the ℓ th Legendre component of the scattering cross section for scattering from group g into group g';

$j = \sqrt{-1}$;

ω = frequency (rad/s);

$P_{\ell}(\mu_d)$ = ℓ th ordinary Legendre polynomial evaluated at μ_d;

L = maximum order of scattering anisotropy;

D = total angular segments;

G = total energy groups;

M = total delayed energy groups.

TASK employs a combination scattering and transfer matrix method with outer (source) iterations to eliminate difficulties arising from round-off and truncation errors. As such, within-group (inner) iterations are eliminated. A complete discussion of the numerical methods embodied in TASK are contained in ref. 1.

APPENDIX A REFERENCES

1. A. R. Buhl et al., "A User's Manual for TASK, a Generalized One-Dimensional Transport and Diffusion Kinetics Code," ORNL-TM-3811 (1972).

2. G. I. Bell and S. Glasstone, *Nuclear Reactor Theory*, New York: Van Nostrand Reinhold Co. (1970).

APPENDIX B

TWO-DIMENSIONAL FREQUENCY-DEPENDENT DIFFUSION THEORY DETECTOR ADJOINT EQUATIONS WITH DELAYED NEUTRONS IN THE JPRKINETICS COMPUTER CODE

APPENDIX B

TWO-DIMENSIONAL FREQUENCY-DEPENDENT DIFFUSION THEORY DETECTOR ADJOINT EQUATIONS WITH DELAYED NEUTRONS IN THE JPRKINETICS COMPUTER CODE

In this appendix, the adjoint multidimensional frequency-dependent kinetics equations solved in the JPRKINETICS computer code are derived.[1] These equations are based on a P_1 approximation to the Boltzmann transport equation (Eq. 4 of Sect. 3).

The adjoint space-, time-, and neutron-energy dependent P_1 equations are:[2]

$$- \nabla\phi_1^{+g}(r,t) - \Sigma_t^g(r,t)\phi_o^{+g}(r,t) + \sum_{g'=1}^{NFG} \Sigma_{s_o}^{g\to g'}(r,t)\phi_o^{+g'}(r,t)$$

$$+ \frac{1}{v_g(r,t)} \frac{\partial\phi_o^{+g}(r,t)}{\partial t} = - S_o^{+g}(r,t) \qquad \text{(B-1)}$$

$$\nabla\phi_o^{+g}(r,t) + 3\,\Sigma_t^g(r,t)\,\phi_1^{+g}(r,t) - 3 \sum_{g'=1}^{NFG} \Sigma_{s_1}^{g\to g'}(r,t)\phi_1^{+g'}(r,t)$$

$$- \frac{3}{v^g(r,t)} \frac{\partial\phi_1^{+g}(r,t)}{\partial t} = 3\, S_1^{+g}(r,t) \qquad \text{(B-2)}$$

where

ϕ_o^{+g} = isotropic component of the adjoint directional flux for group g,

ϕ_1^{+g} = anisotropic component of the adjoint directional flux for group g,

$\Sigma_{s_o}^{g\to g'}$ = isotropic component of the scattering cross section from group g into group g′,

V^g = neutron velocity for group g,

NFG = total number of fine neutron energy groups.

By assuming that the adjoint sources are isotropic, $S_1^{+g}(r,t) = 0$ and the isotropic adjoint source $S_o^{+g}(r,t)$ can be expanded:

$$S_o^{+g}(r,t) = S_{o\,\text{prompt}}^{+g}(r,t) + S_{o\,\text{delayed}}^{+g}(r,t) + S_{o\,\text{external}}^{+g}(r,t) . \qquad \text{(B-3)}$$

Each of the terms in Eq. B-3 can be further expanded:

$$S_{o\,\text{prompt}}^{+g}(r,t) = \sum_{g'=1}^{NFG} \nu\Sigma_f^g(r,t)\chi^{g'}(r,t)\left[(1 - \sum_{i=1}^{NFD} \beta^i(r,t)\right]\phi_o^{+g'}(r,t) \qquad \text{(B-4)}$$

$$S_{o\,\text{delayed}}^{+g}(r,t) = \sum_{g'=1}^{NFG} \sum_{i=1}^{NFD} \gamma^{i\to g'}(r,t)\ \lambda^i(r,t)\ C^{+i}(r,t) \qquad \text{(B-5)}$$

$$S_{o\,\text{external}}^{+g}(r,t) = \Sigma_d^g(r,t) \qquad \text{(B-6)}$$

where

$\nu\Sigma_f^g$ = number of neutrons per fission times the fission cross section for group g,

$\chi^{g'}$ = fraction of prompt neutrons born in group g′,

β^i = fraction of fission neutrons emitted as delayed neutrons of type i,

$\gamma^{i\to g'}$ = fraction of delayed neutrons of type i decaying into group g′,

λ^i = decay constant for delayed neutrons of type i,

Σ_d^g = dectector response function for group g,

NFD = number of fine delayed groups,

C^{+i} = the adjoint delayed neutron density for type i.

By requiring that $C^{+i}(r,t)$ and $C^i(r,t)$ (the "forward" delayed neutron density) vanish on the external boundaries, the adjoint equation for delayed neutrons is

$$\nu\Sigma_f^g(r,t)\ \beta^i(r,t)\ \gamma^{i\to g'}(r,t)\ \phi_o^{+g'}(r,t)\ C^{+i}(r,t) = \frac{-\partial C^{+i}(r,t)}{\partial t} \qquad \text{(B-7)}$$

Using a "modified consistent" (inscatter) approximation, the transport cross section $\Sigma_{tr}^{G\to G'}(r)$, is defined by the solution of:

$$\Sigma_{tr}^{G\to G'}(r) \sum_{g=L_G}^{U_G} \phi_1^{+g}(r) = \sum_{g=L_G}^{U_G'} \left(\Sigma_t^g(r)\ \phi_1^{+g}(r) - \sum_{g'=L_{G'}}^{U_{G'}} S_1^{g\to g'}\ \phi_1^{+g'}(r) \right) \qquad \text{(B-8)}$$

where L and U are the lower and upper fine-energy group boundaries respectively of broad-energy groups G or G', and $\phi_1^+(r)$ are obtained from a static discrete ordinate cell or zone calculations.

Similarly for other variables,

$$V^G(r) = \frac{\sum_{g=L_G}^{U_G} \frac{\phi_o^{+g}(r)}{V^g(r)}}{\sum_{g=L_G}^{U_G} \phi_o^{+g}(r)} \tag{B-9}$$

$$\Sigma_t{}^G(r) = \frac{\sum_{g=L_G}^{U_G} \Sigma_t^g(r)\, \phi_o^{+g}(r)}{\sum_{g=L_G}^{U_G} \phi_o^{+g}(r)} \tag{B-10}$$

$$\nu\Sigma_f{}^G(r) = \frac{\sum_{g=L_G}^{U_G} \nu\Sigma_f^g(r)\, \phi_o^{+g}(r)}{\sum_{g=L_G}^{U_G} \phi_o^{+g}(r)} \tag{B-11}$$

and χ^G and β^I are defined in Appendix C.

By Fourier transforming Eqs. B-1 and B-2 and substituting Eqs. B-3 and B-11, the broad energy-group detector adjoint equation is obtained:

$$\sum_{G'=1}^{NG} \nabla DD^{G\to G'}(r,\omega)\, \nabla\phi^{+G'}(r,\omega) - \left(\Sigma_t^G(r) - \Sigma_{s_o}^{G'\to G}(r) + \frac{j\omega}{V^G(r)}\right) \phi^{+G}(r,\omega)$$

$$+ \sum_{\substack{G'=1 \\ G'\neq G}}^{NG} \Sigma_{s_o}^{G\to G'}(r)\, \phi^{+G'}(r,\omega) + \nu\Sigma_f^G(r) \sum_{G'=1}^{NG} \chi^{G'}(r) \left(1 - \sum_{I=1}^{NDG} \beta^I(r)\right) \phi^{+G'}(r,\omega)$$

$$+ \nu\Sigma_f^G \sum_{I=1}^{NDG} \frac{\beta^I(r)\lambda^I(r)}{\lambda^I(r) + j\omega} \sum_{G'=1}^{NG} \gamma^{I\to G'}\, \phi^{+G'}(r,\omega) = -\Sigma_d^G(r,\omega) \tag{B-12}$$

where

$$DD^{G\to G'}(r,\omega) = 3\left[\Sigma_{tr}^{G\to G'}(r) + \frac{j\omega}{V^{G}(r)}\ \delta(G-G')\right] , \qquad \text{(B-13)}$$

and

$j = \sqrt{-1}$,

ω = frequency (rad/s),

NG = number of broad energy groups,

NDG = number of broad delayed energy groups.

Iterative Procedure

The adjoint Eq. B-13 was solved with the JPRKINETICS computer code.[1] The real and imaginary parts of Eq. (B-13) are solved as coupled energy groups (i.e., three neutron energy groups yield three real and three imaginary equations). Iterative techniques such as constraint block overrelaxation, inner iterations, σ_1 sweep ordering, optimized overrelaxation coefficients, and external source scaling are utilized to obtain an efficient solution to these equations. A detailed description of the calculation techniques is available in ref. 2.

APPENDIX B REFERENCES

1. J. P. Renier, *Multi-Group, Multi-Dimensional Investigations of the Power Spectral Densities of the Georgia Tech Research Reactor and the fast Thermal Argonaut Reactor*, Ph.D. dissertation, Georgia Institute of Technology (1976).

2. J. P. Renier and F. J. Sweeney, "A Method to Calculate Detector Kinetic Sensitivities to In- and Ex-Core Perturbations of Power Reactors," ISBN-0-89448-11-8, ANS Topical Meeting on Advances in Reactor Computations, Salt Lake City, (March 1983).

APPENDIX C

GENERATION OF MULTIGROUP CROSS SECTIONS AND DELAYED-NEUTRON PARAMETERS

APPENDIX C

GENERATION OF MULTIGROUP CROSS SECTIONS AND DELAYED NEUTRON PARAMETERS

The nuclear analysis package used in this study is based on several computational modules developed at ORNL. These modules are called in the proper sequence by JPCYCLE[1-4] to generate:

- weighted multigroup cross sections for the fuel rods, water, burnable poison rods (BPR), control rods, and structural materials, all as a function of fuel material enrichments, fuel burnup, soluble boron concentration of the water, and BPR burnup.

- neutron spectrum-weighted and zone-dependent delayed neutron parameters and neutron group velocities as a function of spatial fuel enrichment, fuel burnup, and soluble boron concentration in the water.

- few-group multidimensional core calculations of the flux, power density, fuel depletion, and BPR depletion, and soluble boron concentration criticality searches.

Figure C-1 displays an overall block diagram of the JPCYCLE driver. Note that it shows only those modules which were used in this study, several of which are not the standard released versions (e.g., CSAS2, XSDRN, NITAWL, DVENTR, DUTLIN). They have been extensively modified within the JPCYCLE modular code system.

1. GENERATION OF THE CROSS SECTIONS

Figure C-2 displays the flow diagram for the generation and update of the burnup-dependent neutron cross sections and the delayed neutron precursor data.

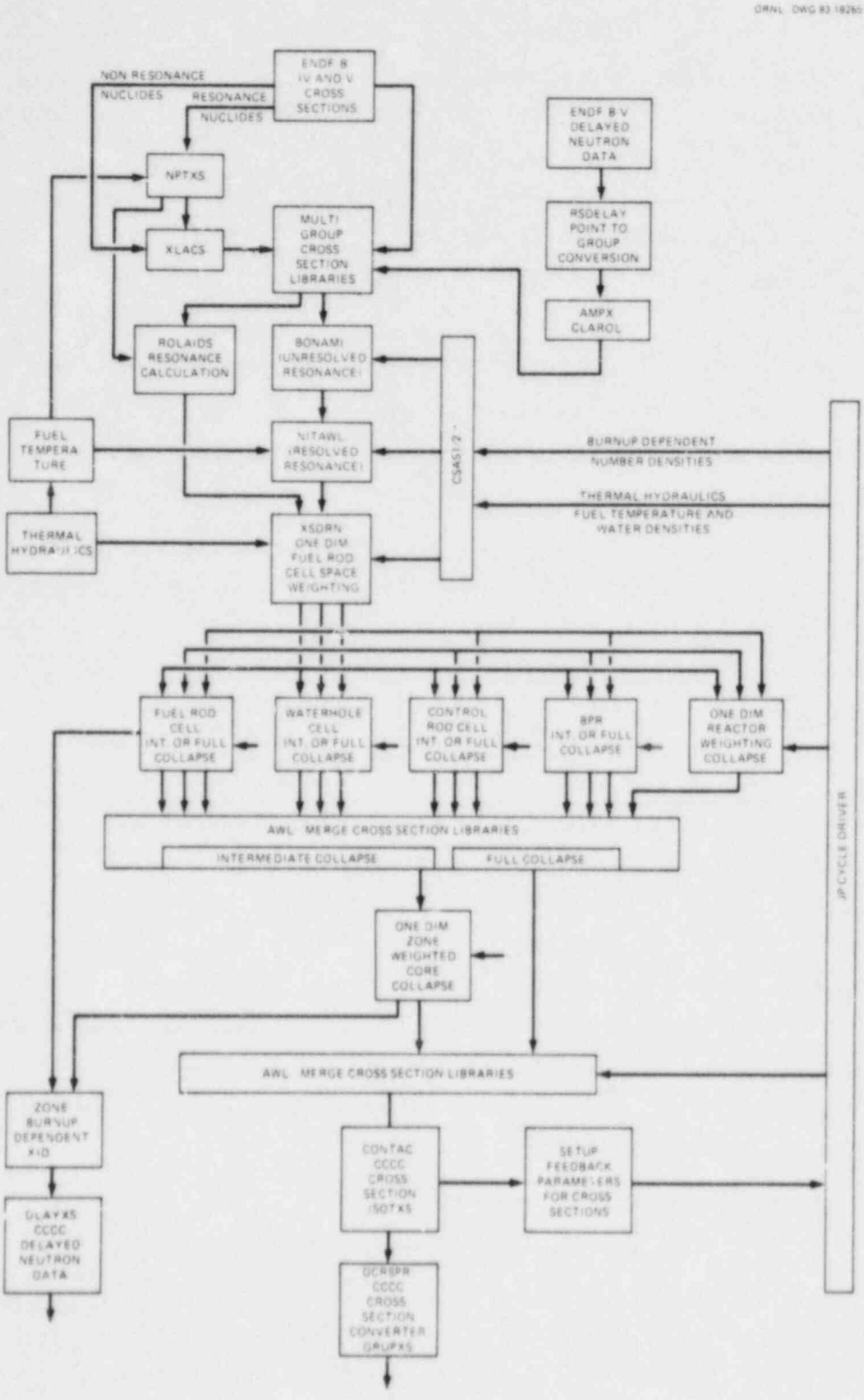

Fig. C-1. Overall block diagram of the JPCYCLE drives.

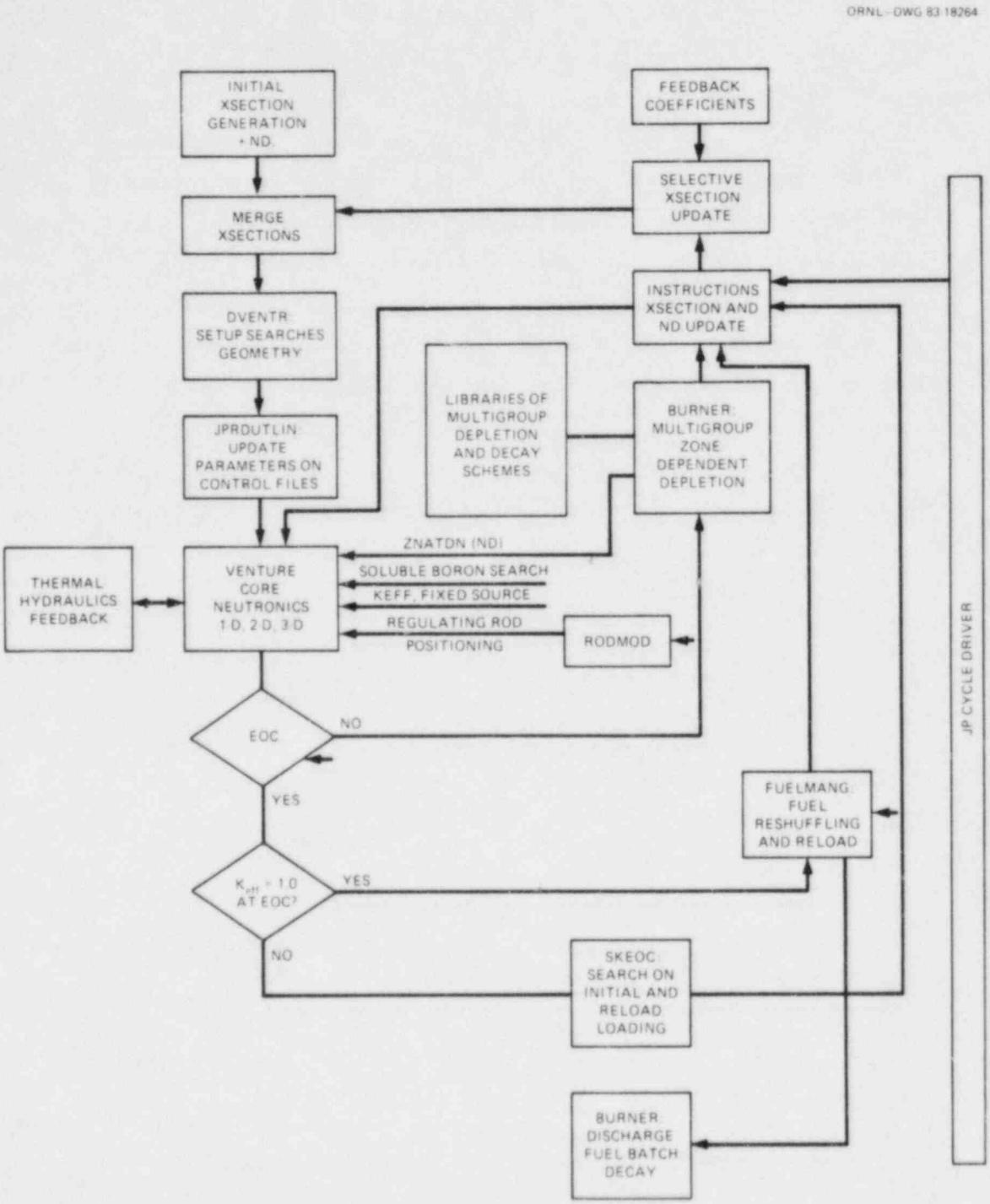

Fig. C-2. Flow diagram for the genreation and update of the burnup-dependent neutron cross sections and the delayed neutron precursor data.

The multigroup cross-section data used in this study were taken from a 27-neutron-energy-group cross-section library in "AMPX Master Library" format. This library contains neutron cross sections which have been generated by collapsing the CSRL (Criticality Safety Reference Library based on ENDF/B-V data)[5,6] 27-fine-neutron-energy-group library to a 27-neutron-energy-group structure using a thermalized spectrum. The CSRL-V library contains cross sections for application to reactor core and shielding analyses and general criticality safety analyses. The majority of the isotopes were obtained previously from ENDF/B-V data using the XLACS-II module of AMPX-II. A few isotopes were processed through modules of NJOY from ENDF/B-V point cross-section data.

The energy structure of the 27-neutron-energy-group library is shown in Table C-1. It has 13 neutron groups with upscattering in the thermal range.

Table C-1. Energy boundaries of the 27-neutron-group cross-section library

Group	Energy Boundaries (MeV)	Energy Group Boundaries (MeV)	
1	2.000E+7	15	3.050E+0
2	6.434E+6	16	1.770E+0
3	3.000E+6	17	1.300E+0
4	1.850E+6	18	1.130E+0
5	1.400E+6	19	1.000E+0
6	9.000E+5	20	8.000E-1
7	4.000E+5	21	4.000E-1
8	1.000E+5	22	3.250E-1
9	1.700E+4	23	2.250E-1
10	3.000E+3	24	1.000E-1
11	5.500E+2	25	5.000E-2
12	1.000E+2	26	3.000E-2
13	3.000E+1	27	1.000E-2
14	1.000E+1		1.000E-5

1.1 GENERATION OF THE CROSS SECTIONS FOR THE FUEL ROD CELLS

The following functional sequence of calculations was performed for each of the three different types of fuel assemblies (low, medium, and high enrichments, called respectively types 3, 2, and 1):

a. For a fuel rod cell of each fuel assembly type, the BONAMI-2 module was used to compute multigroup neutron cross sections in the unresolved resonance region by using the Bondarenko or shielding factor method.[7]

b. For a fuel rod cell of each fuel assembly type, the NITAWL module was used to compute multigroup cross sections in the resolved resonance region by using the Nordheim Integral Method (NIM).[8] Resonance calculations were performed for the isotopes ^{235}U, ^{238}U, and Zr at the beginning of cycle (BOC). In addition, for fuel with burnup a resonance correction is normally made for the principal resonance nuclei. For the core calculations at hot full power (HFP), the resonance corrections were performed at an effective fuel pellet temperature of 1500°K in order to account for Doppler broadening.

c. For a fuel rod cell of each of the fuel assembly types, a multigroup one-dimensional S_8P_3 discrete ordinates transport calculation was performed in cylindrical geometry, followed by a spatial weighting of the cross sections over the cell. A 27-neutron-group fuel-rod-cell weighted cross-section library was thus created. In addition, a cell-weighted collapse of the fuel rod cell to three broad energy groups (boundaries: 20 MeV, 10 keV, 0.625 eV, 0.0 eV) was performed.

A modified version of the discrete ordinates code XSDRN[3] was used. In addition to the capabilities of the standard version of XSDRN, this modified version can calculate zone-dependent and spectrum-weighted values for the prompt fission neutron spectrum χ^G, neutron group velocities, delayed neutron spectrum γ^{I+G}, and delayed neutron fractions β^I.

The fuel rod cell had a reflective boundary conditions. The outer dimension of the cell was chosen such that the H_2O/UO_2 volumetric ratio was conserved.

The following materials and dimensions were used for the fuel cell calculations: UO_2 stack density of 95% TD (theoretical density), pellet diameter 0.3255 in. OD; diametrical gap 0.0075 in.; Zircalogy clad 0.0225 in. thick; cell diameter 0.560 in. OD; H_2O at 570°F and 2235 psi, containing the appropriate (calculated) content of soluble boron; active fuel height 144 in.

1.2 GENERATION OF THE EFFECTIVE DELAYED NEUTRON PARAMETERS

Zone- and isotope-dependent prompt neutron spectra, delayed-neutron spectra, and delayed-neutron fractions were used in the calculations of the multigroup multidimensional frequency-dependent weighting factors.

Since stochastic processes introduce small variations of the fluxes around their respective mean, the broad-group weighted neutron spectra and delayed-neutron parameters will be derived based on steady-state fluxes.

Since on the average the delayed neutrons are born at lower energies than prompt neutrons, two different approaches have been used in the generation of the delayed-neutron parameters:

1. In Appendix B it was shown that the space and energy-dependent transfer functions are obtained by the simultaneous solution of prompt and delayed-neutron equations. If the prompt-neutron spectra χ^G are used instead of the delayed neutron spectra $\gamma^{I \to G'}$ in the delayed-neutron equations, the delayed neutron fractions and prompt neutron spectra have to be adjusted.

The forward, steady-state prompt- and delayed-neutron sources for fine-energy group g, and fissionable isotope z, are given by:

$$S(r)^g_{z\ \text{prompt}} = \sum_{g'=1}^{NFG} \chi_z^{g'}(r) \left(1 - \sum_{i=1}^{NFD} \beta_z^i(r)\right) \nu\Sigma_{f_z}^{g'}(r) \phi_o^{g'}(r) \qquad \text{(C-1)}$$

$$S(r)^g_{z\ \text{delayed}} = \sum_{g'=1}^{NFG} \sum_{i=1}^{NFD} \gamma_z^{i\to g}(r)\, \nu\Sigma_{f_z}^{g'}(r)\, \phi_o^{g'}(r)\, \beta_z^i(r) \qquad \text{(C-2)}$$

where

$\beta_z^i(r)$ = delayed-neutron fraction of delayed-neutron group i due to fission in isotope z,

$\nu\Sigma_{f_z}^{g'}(r)$ = ν times fission cross-section of neutron of energy g′ for fissionable isotope z,

$\gamma_z^{i\to g}(r)$ = spectrum of delayed neutrons due to fission of isotope i,

$\phi_o^{g'}(r)$ = forward steady-state flux of neutron energy group g′.

If the prompt-neutron spectra χ^G is used in the delayed-neutron equations, then the effective broad-group, zone-dependent delayed-neutron fractions for each of the fissionable isotopes z are given by:

$$\beta_{z\ \text{effective}}^I(\text{zone}) = \frac{\displaystyle\int_{\text{zone}} \sum_{g=L_G}^{U_G} \sum_{i=L_I}^{U_I} \gamma_z^{i\to g}(r)\, \nu\Sigma_{f_z}^{g}(r)\, \phi_o^{g}(r)\, \beta_z^i(r)\, d^3r}{\displaystyle\int_{\text{zone}} \sum_{g=L_G}^{U_G} \sum_{g'=L_{G'}}^{U_{G'}} \chi_z^{g}(r)\, \nu\Sigma_{f_z}^{g'}(r)\, \phi_o^{g'}(r)\, d^3r} \qquad \text{(C-3)}$$

where

G and G′ are the broad energy groups,

g and g′ are the fine energy groups,

z is fissionable isotope z.

The effective broad-group zone-dependent neutron spectrum is given by:

$$\chi^{G}(\text{zone}) = \frac{\int_{\text{zone}} \sum_{z} \sum_{g=L_G}^{U_G} \sum_{g'=L_{G'}}^{U_{G'}} \chi_z^{g}(r) \left(1 - \sum_{i=1}^{NFD} \beta_z^{i}(r)\right) \nu\Sigma_{f_z}^{g'}(r)\phi_o^{g'}(r)d^3r}{\int_{\text{zone}} \sum_{z} \sum_{g=L_G}^{U_G} \left(1 - \sum_{i=1}^{NFD} \beta_z^{i}(r)\right) \nu\Sigma_{f_z}^{g}(r)\,\phi_o^{g}(r)d^3r} \qquad \text{(C-4)}$$

2. If the delayed neutron spectra $\gamma^{I\to G}$ are used in the delayed neutron equations, (see Appendix B) then the broad-group, zone-dependent delayed neutron fractions for each of the fissionable isotopes z, using forward flux weighting, are given by:

$$\beta_z^{I}(\text{zone}) \cdot \gamma_z^{I\to G} = \int_{\text{zone}} \sum_{i=L_I}^{U_I} \sum_{g=L_G}^{U_G} \gamma_z^{i\to g}(r)\ \nu\Sigma_{f_z}^{g}(r)\ \phi_o^{g}(r)\ \beta_z^{i}(r)d^3r \qquad \text{(C-5)}$$

The broad-group zone-dependent prompt neutron spectra, using forward flux weighting, are given by Eq. C-4.

The fine-group delayed-neutron parameters $\gamma_z^{i\to g}(r)$, $\beta_z^{i}(r)$ and $\lambda_z^{i}(r)$ for the different fissionable isotopes (^{235}U, ^{238}U, ^{239}Pu, ^{241}Pu) were

obtained from ENDF/B-V point data files. The point data were transformed into the 27-neutron-energy-group structure (see Table C-1) using the RSDELAY module of JPLCYCLE.[1] The fine-group-dependent delayed-neutron parameters were then added into the 27-neutron-energy-group AMPX "Master Cross-Section File" structure using the CLAROL module of AMPX.[2] Since no point data for the delayed parameters of ^{240}Pu and ^{242}Pu were available in the ENDF/B-V files, they were taken to be the same as the ^{239}Pu delayed parameters.

The delayed-neutron parameters were then cell- or zone-weighted (at the same time as the cross sections) using the revised version of the XSDRN module of SCALE. The two approaches were implemented in this version.

The broad-group weighted neutron spectrum and delayed parameters of the second approach were used in all calculations of the space-, energy- and frequency-dependent weighting factors (Eqs. C-5 and C-6). Several calculations were also performed using the first approach and were compared with the second one. The difference in the weighting factors was less than 4% at a frequency of 3 cycles/s.

1.3 GENERATION OF THE CROSS SECTIONS FOR THE BPR

Based on the number and on the location of the BPR, the fuel assemblies containing BPRs can be subdivided into five different types: fuel assemblies of type 1 containing 10, 12, or 16 BPRs; and fuel assemblies of type 2 containing 16 or 20 BPRs.

Two different sets of BPR cross sections were generated, one for the BPRs of type 1 fuel assemblies containing 16 BPRs, and one for the BPRs of type 2 fuel assemblies containing 16 BPRs. The type 1 BPR cross sections were then used for the BPRs in the type 1 fuel assemblies containing 10, 12 or 16 BPRs; and the type 2 BPR cross sections were used for the BPRs and the type 2 fuel assemblies containing 16 or 20 BPRs.

The following calculational sequence was performed to obtain each set of BPR cross sections:

For a BPR cell surrounded by a homogenized type 1 or 2 fuel mixture, multigroup one-dimensional S_8P_3 discrete ordinates transport calculations were performed in cylindrical geometry, followed by a spatial weighting of the cross sections over the cell. A 27-neutron-group BPR cell-weighted cross-section library was thus created. In addition, a cell-weighted collapse of the BPR cell to 3 broad-energy-groups was done in order to generate a 3 broad-energy-group weighted cross-section library for the BPRs and the surrounding water. The BPRs used in the calculations were of the "dry" variety. The BPR cell and surrounding homogenized fuel had reflective boundary conditions.

The following materials and dimensions were used in the generation of the BPR cross sections: vacuum with an OD of 0.1685 in.; SS-304 inner tube with an OD of 0.1805 in. and a wall thickness of 0.006 in.; borosiliate glass (B_2O_3 in glass) in an annualar form, with a boron loading of 0.00042 lb B^{10} per foot of rod; outer SS-304 tube with an OD of 0.381 in., and a wall thickness of 0.0185 in.; H_2O at 570°F and 2235 psi with soluble boron and an OD of 0.418 in.; Zircaloy-4 guide tube of 0.482 in. OD; H_2O at 570°F and 2235 psi, containing the appropriate (calculated) content of soluble boron, and with an outer diameter chosen such that the H_2O/BPR volumetric ratio was conserved; homogenized fuel-clad-water mixture with an outer diameter such that the fuel-rod-cell/BPR-cell volumetric ratio in the fuel assembly was conserved.

The cross sections for the homogenized fuel-clad-water mixtures were obtained from the 27-neutron-group fuel-rod-cell spatial-weighted library for fuel assembly types 1, and 2 (see Sect. C.1.1). The 27-neutron-group cross sections for the other materials (BPR cladding borosilicate glass, water and soluble boron) were obtained from the 27-neutron-group ENDF/B-V AMPX master libraries and treatment through the NITAWL module. The two sets of BPR cross sections were merged using the AWL module of AMPX.

1.4 GENERATION OF THE CROSS SECTIONS FOR THE WATERHOLES

The following calculational sequence was performed in the generation of the cross sections for the waterholes of the three different types of fuel assemblies:

For a waterhole cell surrounded by homogenized fuel mixture of type 1, 2, or 3, a multigroup one-dimensional S_8P_3 discrete ordinates transport calculation was performed in cylindrical geometry, followed by a spatial weighting of the cross sections over the waterhole cell. A 27-neutron-group waterhole cell-weighted cross-section library was thus created. In addition, a cell-weighted collapse of the BPR cell to three broad energy groups was also performed in order to generate a three broad-energy-group weighted cross-section library for the waterholes.

The following materials and dimensions were used in the generation of the waterhole cross sections: H_2O at 570°F and 2235 psi, containing soluble boron and with an OD of 0.450 in.; Zircaloy-4 guide tube, 0.482 in. OD; H_2O at 570°F and 2235 psi, containing the appropriate (calculated) content of soluble boron and with an outer diameter of 0.560 in.; homogenized fuel-clad-water mixture of type 1, 2, or 3 with an outer diameter such that the fuel-rod-cell/waterhole volumetric ratio in the fuel assembly was conserved (e.g., 25 waterholes per type 1 fuel assembly). The different sets of waterhole cross sections were merged using the AWL module of AMPX.

1.5 GENERATION OF THE CROSS SECTIONS FOR THE EX-CORE MATERIALS

The following calculational sequence was performed on the generation of the zone-dependent and collapsed cross sections for the different ex-core regions. These ex-core regions were the core liner, water-steel reflector, core barrel, water gap, thermal shield, downcomer, reactor vessel, and biological shield.

A one-dimensional S_8P_3 discrete ordinates transport eigenvalue calculation was performed in cylindrical geometry using the cell-weighted 27-neutron-group libraries previously created. This was followed by a zone-weighted collapse of the cross sections and of the neutron velocities in the ex-core regions from 27-neutron-energy groups to three broad groups, using the revised version of XSDRN.

The following materials, dimensions, and cross-section libraries were used in the generation of the ex-core region cross sections. The checkerboard pattern of the different types of fuel assemblies in the core was simulated with different concentric cylinders containing homogenized fuel assemblies, each with a thickness of 8.466 in. The homogenized number densities (HND) were based on 264 fuel rods per assembly. Starting from the center of the core, the HND of the fuel assemblies were based on: type 3 fuel assembly with 25 waterholes; type 2 with 20 BPR and 9 waterholes; type 3 with 25 waterholes; type 2 with 16 BPR and 9 waterholes; type 3 with 25 waterholes; type 1 with 10 BPR and 15 waterholes.

For each of the zones, the 27-neutron-energy-group cell-weighted cross-section libraries for the fuel rod cell, BPR cell and waterhole cell were used. The generation of these weighted libraries was described in previous sections.

The following materials and dimensions were used outside the core: core liner, 0.75 in. thick; water-steel reflector with 10% steel and water at 570°F and 2235 psi, with the appropriate amount of soluble boron and 148 in. OD; core barrel, carbon steel, 2.25 in. thick and 152.5 in. OD; water gap, 3 in. thick, 158.5 in. OD, containing H_2O with soluble boron; thermal shield, 2.75 in. thick, 164 in. OD and carbon steel; downcomer, 4.5 in. thick, 172.5 in. OD, containing H_2O with soluble boron; reactor vessel, 8.375 in. thick, 189.75 in. OD and carbon steel; air gap, 10 in. thick; biological shield, 11.625 in. thick, 233.0 in. OD and Oak Ridge concrete. For the ex-core regions, the 27-neutron-energy-group

AMPX master cross section files were used. The resonance calculations were performed with the NITAWL module of SCALE.

A one-dimensional S_8P_3 discrete ordinates transport eigenvalue calculation for the core and ex-core regions, using the revised version of the XSDRN module of SCALE, was performed in order to generate 27-neutron-group fluxes. A zone-weighted collapse of the ex-core material cross sections and neutron group velocities to three broad-energy-groups was then performed using this revised XSDRN module.

These zone-weighted collapsed cross sections for the ex-core regions were merged with the cell-weighted collapsed cross sections for the fuel-rod cells, BPR cells and waterhole cells, using the AWL module of AMPX. This merged cross-section library was then converted into a CCCC-compatible (DOE Committee on Computer Code Coordination) nuclide-ordered ISOTXS multigroup cross-section file, using a revised version of the CONTAC module of AMPX. This nuclide-ordered cross section file was then converted to an energy-group-ordered GRUPXS file using the CROSPROS module of BOLDVENTURE.[4]

The individual energy releases for the various neutronic reactions (e.g., n-γ, n-f) in each isotope were specifically taken into account in the calculations of the reactor power. Values of 194.0, 198.1, 200.0, and 202 MeV/fission were used for ^{235}U, ^{238}U, ^{239}Pu, and ^{241}Pu respectively.[9]

2. MULTI-DIMENSIONAL REACTOR CORE CALCULATIONS AND FUEL DEPLETION

The reactor core calculations (k_{eff}, soluble boron concentration searches) were performed using the VENTNEUT neutronics module of BOLD-VENTURE.[4] The diffusion calculations were performed in the xy-geometry. The depletion calculations were performed with the BURNER module of BOLD-VENTURE, using a total of 50 isotopes on the depletion chains. The first core cycle was subdivided into 7 depletion time steps. At each depletion time step, a soluble boron concentration search was performed. The cross sections were updated at every other depletion time step.

Since the generation of the cross sections for the core and ex-core regions depends on the amount of soluble boron in the water, an iteration was performed at the initial time step. This iteration step included generation of the cross sections and a soluble boron search until the change in soluble boron concentration was less than 1%.

Figure C-3 displays the flow diagram for the multidimensional steady-state neutronics, depletion, soluble boron searches, control rod positioning, and burnup-dependent cross-section calculations.

In order to reduce computer time requirements, the steady-state neutronics analyses were performed using a quarter-core geometry with two reflective boundaries and two zero boundaries. The reactor fuel region was surrounded by a reflector approximately 8 in. thick containing water at 570°F and 2235 psi, an appropriate amount (calculated through a criticality search) of soluble boron, and approximately 10% steel. The fuel depletion calculations were performed using a 1/8-core geometry. The neutronics calculations were performed for a core containing BPRs and for a core where the BPRs were replaced with waterholes. In all of the calculations at hot-full-power (HFP), all regulating control rods were in a fully withdrawn position.

Figure C-4 displays the results of the soluble boron searches as a function of fuel exposure time in full-power-days (FPD), with and without BPRs.

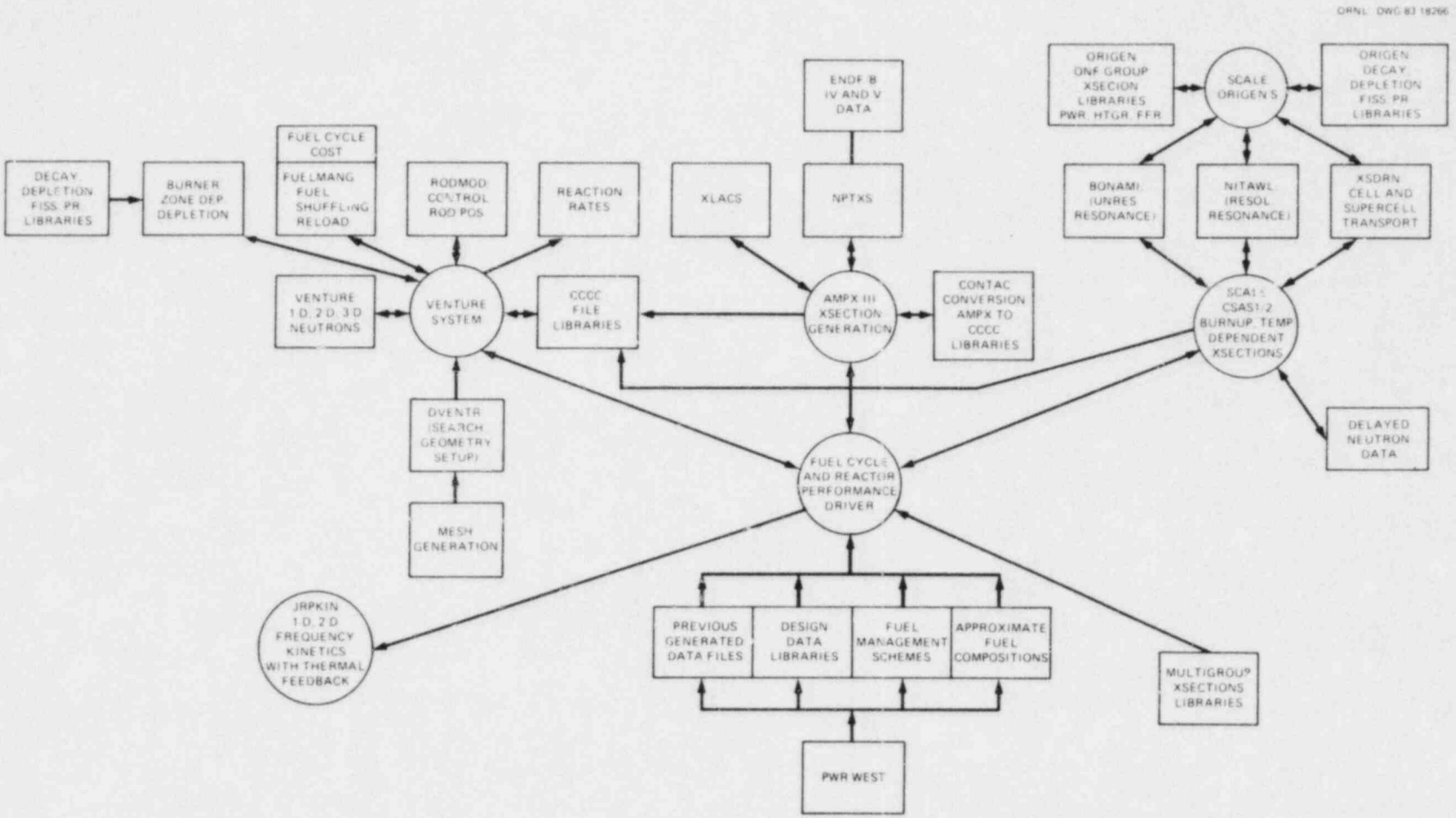

Fig. C-3. Flow diagram for the multidimensional steady-state neutronics, depletion, soluble boron searches, control rod positioning, and burnup-dependent cross-section calculations.

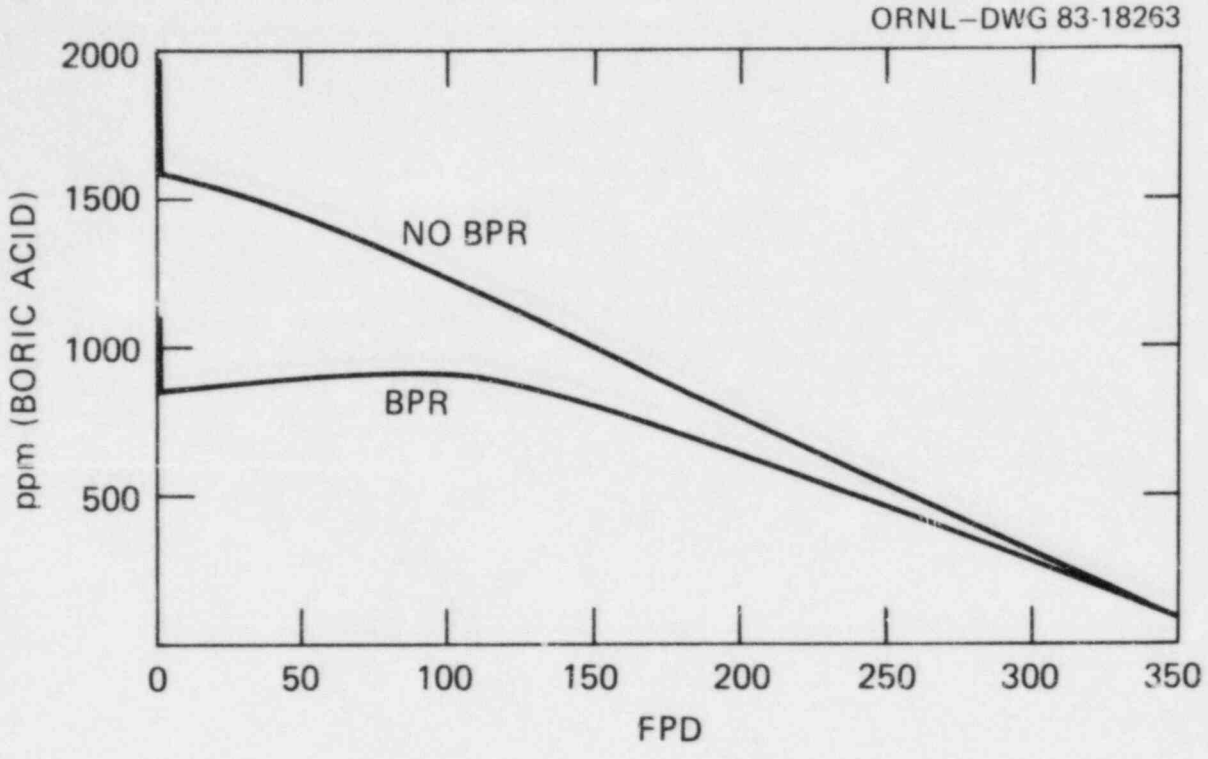

Fig. C-4. Calculated soluble boron concentration as a function of fuel exposure time in full-powered-days (FPD), with and without BPRs.

APPENDIX C REFERENCES

1. J. P. Renier and F. J. Sweeney, "JPCYCLE: A Modular Code System Driver for Performing Reactor Fuel Cycle Calculations Based on the Use of SCALE, VENTURE, and AMPX-II Modules" (to be published).

2. N. M. Greene et al., "AMPX: A Modular Code System for Generating Coupled Multigroup Neutron-Gamma Libraries from ENDF/B," ORNL/TM-3706 (March 1976).

3. R. M. Westfall et al., "SCALE: A Modular Code System for Performing Standarized Computer Analyses for Licensing Evaluation," NUREG/CR-0200 (ORNL/NUREG/CSD-2) Vols. 1-3 (November 1981).

4. D. R. Vondy et al., "BOLD VENTURE: System for Nuclear Reactor Core Analyses, Version III," ORNL-5711 (June 1981).

5. W. E. Ford, III et al., "CSRL-V: An ENDF/B-V 227-Group Cross-Section Library for Criticality Safety Studies," *Trans. Am. Nucl. Soc.* 34, 331 (1980).

6. B. R. Diggs et al., "CSRL-V: Processed ENDF/B-V 227-Neutron-Group and Pointwise Cross-Section Libraries for Criticality Safety, Reactor, and Shielding Studies," NUREG/CR-2306 (to be published).

7. I. I. Bondarenko et al., "Group Constants for Nuclear Reactor Calculations," New York: Consultants' Bureau, 1964.

8. L. W. Nordheim, "The Theory of Resonance Absorption," *Proc. Symposia in Appl. Mathematics,* Vol. XI, pp. 58, Am. Math. Soc. (1961).

9. R. Shu et al., "Fission Energy Release for 16 Fissioning Nuclides," EPRI-NP-1771 (March 1981).

☆U.S. GOVERNMENT PRINTING OFFICE: 1983-746-018/4077

NUREG/CR-2996
ORNL/TM 8549
NRC Distribution R4

INTERNAL DISTRIBUTION

1. M. E. Buchanan
2. B. G. Eads
3-12. D. N. Fry
13. R. C. Gonzalez
14. T. L. King
15. W. T. King
16. R. C. Kryter
17. A. P. Malinauskas
18. J. March-Leuba
19. J. A. Mullens
20. F. R. Mynatt
21. L. C. Oakes
22 R. B. Perez
23-32. J. P. Renier
33. D. Shieh
34. C. M. Smith
35-59. F. J. Sweeney
60. B. R. Upadhyaya
61. R. T. Wood
62. M. J. Kopp (Advisor)
63. P. F. McCrea (Advisor)
64. P. W. Murrill (Advisor)
65. H. M. Paynter (Advisor)
66. H. E. Trammell (Advisor)
67-68. Laboratory Records
69. Laboratory Records, ORNL RC
70-71. Central Researach Library
72. Y-12 Document Reference Sect.
73. ORNL Patent Section
74. I&C Publications Office

EXTERNAL DISTRIBUTION

75. G. Th. Analytis, Swiss Federal Research Institute - EIR, CH-5303, Würenlingen, Switzerland.
76. D. G. Cain, Nuclear Safety Analysis Center, Electric Power Research Institute, 3412 Hillview Ave., P.O. Box 10412, Palo Alto, CA 94304.
77. R. B. Duffey, Electric Power Research Institute, 3412 Hillview Avenue, P.O. Box 10412, Palo Alto, CA 94303.
78. G. B. Fader, Institute of Nuclear Power Operations, 1100 Circle 75 Parkway, Suite 1500, Atlanta, GA 30339.
79. W. S. Farmer, U.S. Nuclear Regulatory Commission, MS-1130SS, Washington, DC 20555.
80. G. P. Horne, Nuclear Engineering Services, Duke Power Company, P. O. Box 33189, Charlotte, NC 28242.
81. R. T. Jones, Philadelphia Electric Co., 2301 Market Street, Philadelphia, PA 19101.
82. N. N. Kondic, U.S. Nuclear Regulatory Commission, MS-NL5650, Washington, DC 20555.
83. G. Kosaly, Department of Nuclear Engineering, The University of Washington, Seattle, WA 98195.
84. G. S. Lewis, Office of Inspection and Enforcement, U.S. Nuclear Regulatory Commission, Washington, DC 20555.
85. L. Lois, U.S. Nuclear Regulatory Commission, MS P-924, Washington, DC 20555.
86. E. L. Machado, IPEN/CNEN RT, C. P. 11049, Pinheros, Sao Paulo, SP 01000 Brazil.

87. J. Royce Maner, Tennessee Valley Authority, Chestnut Street Towers II, Room 740, Chattanooga, TN 37410.
88. C. W. Mayo, Science Applications, Inc., Jackson Plaza Tower, Suite 1000, 800 Oak Ridge Turnpike, Oak Ridge, TN 37830.
89. D. W. Miller, Ohio State University, 206 West 18th Avenue, Columbus, OH 43210.
90. A. Morris, Tennessee Valley Authority, 1300 Chestnut Street Towers II, Chattanooga, TN 37401.
91. C. Puyal, Electricite De France, 6, Quai Watier 78400, Chatou, France.
92. J. C. Robinson, Technology for Energy Corporation, One Energy Center, Pellissippi Parkway, Knoxville, TN 37922.
93. R. F. Saxe, Department of Nuclear Engineering, North Carolina State University, P. O. Box 5636, Raleigh, NC 27607.
94. J. Steelman, Baltimore Gas and Electric Co., Calvert Cliffs Nuclear Station, Lusby Post Office, Lusby, MD 20657.
95. R. Sunder, Gesellschaft für Reaktorsicherheit Forschungsgelände, D-8046, Garching, Federal Republic of Germany.
96. E. Turkcan, Netherlands Energy Research Foundation ECN, 3 Westendurinweg, Petten, The Netherlands.
97. G. Weidenhamer, U.S. Nuclear Regulatory Commission, MS-1130SS, Washington, DC 20555.

98-99. Technical Information Center, Box 62, Oak Ridge, TN 37831.

100-399. Given distribution under NRC Category R-4, Water Reactor Safety Research Analysis Development (NTIS-10 copies).

NRC FORM 335 (11-81)

U.S. NUCLEAR REGULATORY COMMISSION

BIBLIOGRAPHIC DATA SHEET

1. REPORT NUMBER (Assigned by DDC)
NUREG/CR-2996
ORNL/TM-8549

4. TITLE AND SUBTITLE (Add Volume No., if appropriate)
Sensitivity of Detecting In-Core Vibrations and Boiling in Pressurized Water Reactors Using Ex-Core Neutron Noise

2. (Leave blank)

3. RECIPIENT'S ACCESSION NO.

7. AUTHOR(S)
F. J. Sweeney, J. P. Renier

5. DATE REPORT COMPLETED
MONTH January YEAR 1984

9. PERFORMING ORGANIZATION NAME AND MAILING ADDRESS (Include Zip Code)
Oak Ridge National Laboratory
P. O. Box X
Oak Ridge, TN 37831

DATE REPORT ISSUED
MONTH YEAR

6. (Leave blank)

8. (Leave blank)

12. SPONSORING ORGANIZATION NAME AND MAILING ADDRESS (Include Zip Code)
Office of Nuclear Regulatory Research
Division of Engineering Technology
U.S. Nuclear Regulatory Commission
Washington, DC 20555

10. PROJECT/TASK/WORK UNIT NO.

11. FIN NO.
B0191
B0754

13. TYPE OF REPORT
NUREG/CR

PERIOD COVERED (Inclusive dates)

15. SUPPLEMENTARY NOTES

14. (Leave blank)

16. ABSTRACT (200 words or less)

Neutron transport and diffusion theory space- and energy-dependent reactor kinetics calculations were performed in the frequency domain to determine the sensitivity of an ex-core neutron detector to in-core vibrations and coolant boiling in a pressurized water reactor (PWR). The results of these calcualtions indicate that the ex-core detectors are sensitive to neutron sources, to vibrations, and to boiling occurring over large regions of the core. Calculations were also performed to determine the effects of fuel burnup, boron concentration, and xenon poisoning on the spatial sensitivity of the ex-core detector. These calculated results show that fuel assembly vibrations would be expected to produce ~60% greater ex-core detector response at the end of the first fuel cycle at Sequoyah-1 compared to the beginning of the fuel cycle for a constant amplitude of vibration. The results were compared with experimental ex-core neutron noise data obtained from Sequoyah-1 during the first fuel cycle. The predicted increase in ex-core neutron noise was experimentally observed in the 2.5- to 4.0-Hz frequency range (the range of frequencies associated with fuel assembly vibration), indicating that the vibrational amplitude of the fuel assemblies did not increase significantly during the first fuel cycle.

17. KEY WORDS AND DOCUMENT ANALYSIS

17a. DESCRIPTORS

17b. IDENTIFIERS/OPEN-ENDED TERMS

18. AVAILABILITY STATEMENT

19. SECURITY CLASS (This report)

21. NO. OF PAGES

20. SECURITY CLASS (This page)

22. PRICE
$